Check for updates

UPLC-ESI/MSn metabolic profiling of *Cedrela odorata* L. and *Toona ciliata* M. Roem and *in vitro* investigation of their anti-diabetic activity supported with molecular docking studies

Heba A. S. El-Nashar[1]*, Ayman M. Al-Qaaneh [2,3],
Md. Shimul Bhuia[4,5], Raihan Chowdhury[4,5],
Mostafa A. Abdel-Maksoud[6], Hossam Ebaid[7], Abdul Malik[8],
Muhammad Torequl Islam[4,5,9], Mohammed Aufy[10]* and
Esraa A. Elhawary[1]

[1]Department of Pharmacognosy, Faculty of Pharmacy, Ain Shams University, Cairo, Egypt, [2]Department
of Allied Health Sciences, Al-Balqa Applied University (BAU), Al-Salt, Jordan, [3]Department of
Pharmaceutical Technology, Faculty of Pharmacy, Jordan University of Science and Technology (JUST),
Irbid, Jordan, [4]Bioinformatics and Drug Innovation Laboratory, BioLuster Research Center, Dhaka,
Bangladesh, [5]Department of Pharmacy, Bangabandhu Sheikh Mujibur Rahman Science and Technology,
University, Gopalganj, Bangladesh, [6]Botany and Microbiology Department, College of Science, King Saud
University, Riyadh, Saudi Arabia, [7]Department of Zoology, College of Science, King Saud University,
Riyadh, Saudi Arabia, [8]Department of Pharmaceutics, College of Pharmacy, King Saud University, Riyadh,
Saudi Arabia, [9]Pharmacy Discipline, Khulna University, Khulna, Bangladesh, [10]Department of
Pharmaceutical Sciences, Division of Pharmacology and Toxicology, University of Vienna, Vienna, Austria

Introduction: The genus *Cedrela* is one of the phytochemically rich genera of the family Meliaceae. In this study, two *Cedrela* species, namely, *Cedrela odorata* and *Toona ciliata* M. Roem (formerly *Cedrela toona*), were selected for in-depth phytochemical profiling with the aid of UPLC-ESI/MSn analysis followed by evaluation of their anti-diabetic potential through assessment of *in vitro* α-amylase and α-glucosidase inhibitory effects, alongside the molecular docking studies on these target enzymes.

Materials and methods: UPLC-ESI/MSn technique was applied to tentatively identify the extracts. The anti-diabetic properties were assessed using BioVision α-amylase and α-glucosidase inhibitor screening kits. Further, the molecular docking studies utilized PyRx® and Discovery Studio software.

Results and discussion: The UPLC-ESI/MSn analysis led to the identification and quantification of 55 metabolites with their fragmentation patterns for the first time for these two species. Flavonoids represented the main identified class, followed by phenylpropanoids, terpenes, tannins, and others. The two species showed potent enzyme inhibition, where *C. odorata* and *C. toona* significantly inhibited α-amylase (IC_{50} = 4.83 $\pm$ 0.01 and 3.50 $\pm$ 0.03 μg/mL) compared to pioglitazone (IC_{50} = 2.17 $\pm$ 0.23 μg/mL), while their α-glycosidase inhibitory properties were also potent with (IC_{50} = 7.17 $\pm$ 0.01 and 6.50 $\pm$ 0.69 μg/mL), respectively, compared to acarbose (IC_{50} = 4.83 $\pm$ 1.02 μg/mL). The enzyme

inhibitory activities were further confirmed by *in silico* molecular docking of the main identified components with the respective binding sockets in both α-amylase and α-glycosidase enzymes.

Conclusion: These promising results could pave the way for a novel discovery of natural phytoconstituents with potent anti-diabetic activity.

1 Introduction

Diabetes mellitus (DM) is a chronic metabolic disease with increasing prevalence and incidence worldwide at an alarming rate (Kaur et al., 2018; El-Nashar et al., 2024a; Todirascu-Ciornea et al., 2019). The most common type of DM is type-2 diabetes (non-insulin-dependent), which mostly affect adults and accounts for 90% of all diabetes cases (Mukhtar et al., 2020; Abdelghffar et al., 2022). Various oral commercial anti-diabetic drugs like biguanides, meglitinide, sulfonylureas, thiazolidinedione, dipeptidyl peptidase-4 (DPP-4) inhibitors, sodium–glucose cotransporter, and carbohydrate-hydrolyzing enzyme inhibitors have been implemented to control postprandial hyperglycemia (Chaudhury et al., 2017; El-Nashar et al., 2023). Some of the most effective anti-diabetic drugs are α-glucosidase and α-amylase inhibitors used for reducing postprandial hyperglycemia (Derosa and Maffioli, 2012; Saber et al., 2023). The available marketable inhibitors such as acarbose, voglibose, and miglitol competitively inhibit these metabolic enzymes, and thus delay digestion, leading to reduction of carbohydrate absorption and thus constraining postprandial hyperglycemia (Derosa and Maffioli, 2012). These drugs are administrated prior to consumption of complex carbohydrate-rich meals, which reduces the glycated hemoglobin (Hb_{A1c}) levels, but these drugs suffer from frequent gastrointestinal tract (GIT)-related side effects (Godbout and Chiasson, 2007). Accordingly, several scientists are devoted to the discovery of novel α-glucosidase and/or α-amylase inhibitors with fewer or no undesired effects from natural sources (Riyaphan et al., 2021). Nowadays, plant-based medicines and functional foods have generated a renewed interest for the prevention and cure of diabetes, given their few or no side effects (Tundis et al., 2010; Rabie et al., 2023). The plant kingdom offers rich arrays of natural bioactive hypoglycemic agents (Hung et al., 2012; El-Nashar et al., 2021a). In the past few decades, over 1,200 plant species have been empirically used as hypoglycemic agents worldwide (Ervina, 2020; Jamaddar et al., 2023; El-Nashar et al., 2022). Consequently, the natural inhibitors of α-glucosidase and α-amylase from plant sources are considered an attractive strategy for treating hyperglycemia (El-Nashar et al., 2024a; El-Nashar et al., 2021b).

C. odorata is a fast-growing perennial tree with paripinnate leaves, belonging to the family Meliaceae (Cavers et al., 2013). This species originated from Pacific and Atlantic Central America, the

GRAPHICAL ABSTRACT
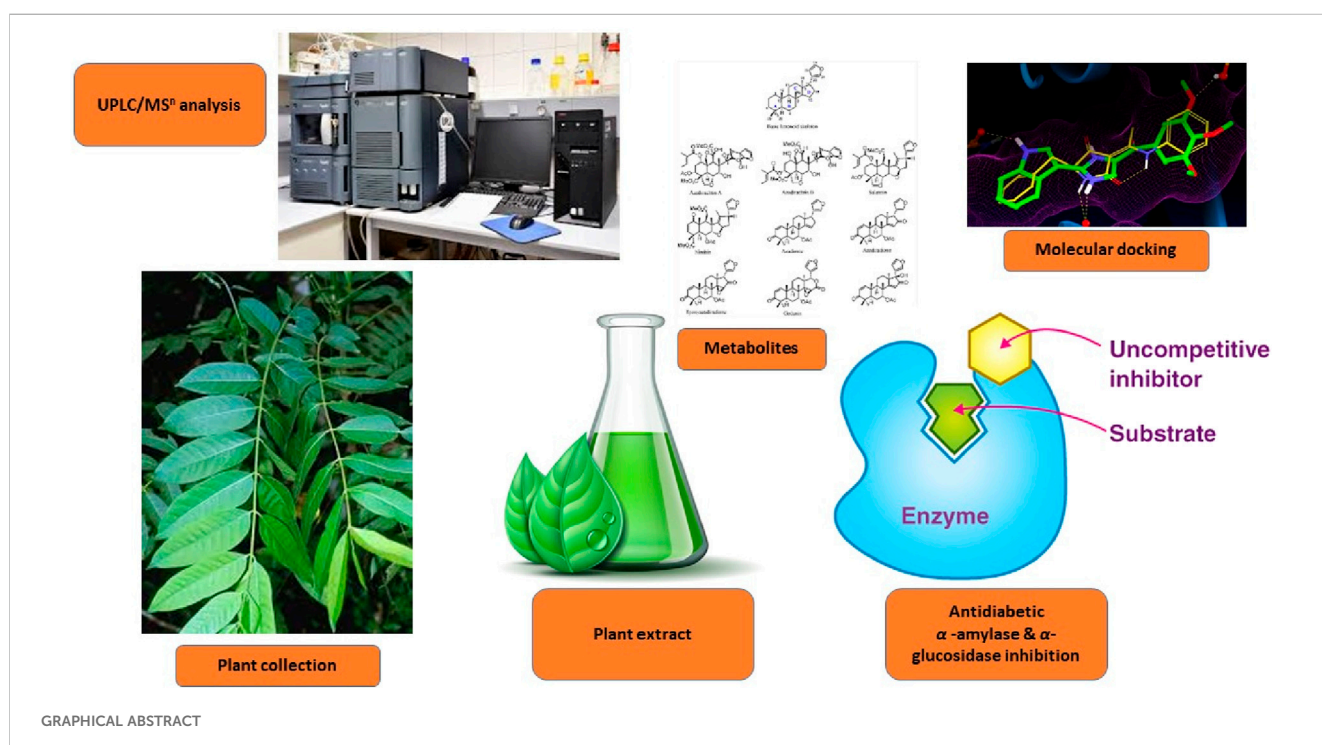
Antilles, South America, both east and west of the Andes, central and eastern coastal Brazil, and northern Argentina. It is a monecious tree, pollinated by small insects with small, wind-dispersed seeds. It grows up to 800 m, but in Ecuador, some trees grow up to 1,500 m (Galván-Hernández et al., 2018). Even though it grows in both evergreen rain forest and drier forest, it can thrive in dry ecological habitats such as deciduous habitat, and buds are protected by scaly leaves (Finch et al., 2022). The fruit takes a long time for maturation in the dry season (Cavers et al., 2013). In folk medicine, the stem bark infusion of *C. odorata* was used for the treatment of fever, hemorrhage, inflammation, and digestive diseases, including diarrhea, vomiting, and indigestion, in South America. The bark decoction was used for as malarial treatment and for fever in Africa. The family Meliaceae and especially genus *Cedrela* are rich in limonoids, alkaloids, and polyphenols such as lignans and proanthocyanidins (Muñoz Camero et al., 2018).

Toona ciliata M. Roem (formerly *Cedrela toona* Roxb.) is a medium- to large-sized deciduous tree with a brown-to-gray scaly bark. Leaves are 15–45 cm long, usually paripinnate, but sometimes with a terminal leaflet; leaflets are mostly 8–20 cm, ovate in shape, 4–15 cm long, 15–50 mm wide, apex acuminate, base strongly asymmetric, margins entire, mostly glabrous, the petiole is 4–11 cm long, and petiolules are 5–12 mm long. The penicles are 20–40 cm long. The petals are 5–6 mm long and white in color. The capsules are ellipsoid, 10–20 mm long, 6–8 mm diameter; seeds are winged at both ends. Traditionally, the bark is reported to be used as astringent, anti-dysenteric, and anti-periodic. Flowers are emmenagogue, and the leaf is spasmolytic, hypoglycemic, and anti-protozoal (Shah and Patel, 2021).

The current study was directed to comparatively analyze the phytoconstituents of the 80% methanol leaf extracts of *Cedrela odorata* and *Toona ciliata* M. Roem via the UPLC-ESI/MS^n technique and investigate α-amylase and α-glucosidase inhibitory properties. Moreover, molecular docking experiments were carried out to assess the binding affinities of plant extract components with the targeted enzymes.

2 Material and methods

2.1 Plant material collection

The fresh leaves of *Cedrela odorata* and *Toona ciliata* were obtained from The Animal Zoo Garden, Dokki, Giza, Egypt (30°01′16.99″N 31°12′30.01″E) in February 2023. The leaves of each species were taxonomically identified by Mrs. Tereize Labib, the taxonomy specialist at El-Orman Botanical Garden, Giza, Egypt. The voucher specimens (PHG-P-CO-482 and PHG-P-CT-481) have been kept for *Cedrela odorata* and *Toona ciliata*, respectively, in the Herbarium of the Pharmacognosy Department, Faculty of Pharmacy, Ain Shams University, Cairo, Egypt.

2.2 Preparation of plant extracts

The fresh leaves of each species (0.5 kg) were finely cut and soaked in 80% aqueous methanol (5 L, BioChem. Comp., Egypt) by percolation at room temperature till depletion. Then, the extracts

were filtrated and concentrated under reduced pressure using a rotavapor (Buchi, R-300) to yield completely dry extracts of *Cedrela odorata* (10.31 gm) and *Toona ciliata* (8.06 gm).

2.3 Ultra-performance liquid chromatography–electrospray ionization-mass spectrometry (UPLC-ESI/MS^n) analysis

UPLC-ESI/MS^n in both positive and negative ion acquisition modes were carried out according to the method adopted from Elhawary et al. (2021).

2.4 Assessment of *in vitro* anti-diabetic activities

2.4.1 α-Amylase inhibition assay

The α-amylase inhibitory activities of the tested *Cedrela* extracts were determined according to the standard published procedure with minor amendments (Kazeem et al., 2013). The enzyme solution was prepared by dissolving α-amylase in 20 mM phosphate buffer (pH = 6.9) at a concentration of 0.50 mg/mL. Then, 1 mL of different concentrations of the tested extract (0.01–100 µg/mL) was mixed with 1 mL of enzyme solution and allowed to sit at room temperature for 10 min. After incubation, 1 mL of 0.50% starch solution was included to the mixture and further incubated at room temperature for 10 min. The reaction was then ended by addition of 3,5-dinitrosalicylic acid (2 mL) and then heating the reaction mixture in a boiling water bath for 5 min. After cooling, the absorbance of the mixture was colorimetrically determined at 565 nm. Pioglitazone was used as a standard drug. The inhibition percentage was calculated using the following formula.

$$\% \text{ inhibition} = (1 - As/Ac) \times 100,$$

where
As = the absorbance of the tested extract and
Ac = the absorbance of the control reaction (containing all reagents except the test sample).

The IC$_{50}$ value was specified as the concentration of the plant extract to inhibit 50% of α-amylase activity under the experiment conditions.

2.4.2 α-Glucosidase inhibition assay

The α-glucosidase inhibitory activities of the plant extracts were determined based on the previously described technique using the BioVision α-glucosidase inhibitor screening kit (K938-100) (El-Nashar et al., 2021b). The tested plant extract (10 µL) was mixed with the same volume of glutathione and α-glucosidase solution (in phosphate buffer (pH = 6.8), and 4-nitrophenyl-α-D-glucopyranoside (10 µL) in a 96-well microplate and incubated for 15–20 min at 25°C. Likewise, the blank solution was prepared by adding the plant extract to all used reaction reagents lacking α-glucosidase solution. The principle of the reaction is based on the ability of an active α-glucosidase to cleave a synthetic substrate (4-nitrophenyl-α-D-glucopyranoside), into a chromophore (p-nitrophenol; OD = 410 nm). Acarbose was used as a standard drug. The reaction was then stopped upon addition of 50 µL of

sodium carbonate (0.2 M). The absorbance of the tested extract and blank was assessed at 410 nm. The absorbance of the blank was subtracted from the values of the tested extract, and the results were stated as IC_{50}.

2.5 *In silico* molecular docking experiments

2.5.1 Ligand preparation

Data of most of the ligands were downloaded from the PubChem® chemical database, while some were drawn using ChemDraw® Professional software. The structures of the chemical compounds were then converted into 3D format and their energy minimized using Chem3D® Pro software, employing the MM2 Allinger's force field method. All ligands were imported as SDF files for conducting the molecular docking study (Bhuia et al., 2023).

2.5.2 Target enzyme collection and preparation

Based on the literature review, it is known that *alpha*-amylase and *alpha*-glucosidase play crucial roles in the pathophysiology of diabetic disorders. The information of the targeted enzymes, *alpha*-amylase (PDB ID: 4GQR) and *alpha*-glucosidase (PDB ID: 3TOP), was obtained from the RCSB Protein Data Bank. Subsequently, the targeted enzymes underwent optimization by removal of water molecules, co-crystal ligands, and unwanted protein chains using Discovery Studio® software (Afroz et al., 2024). Following the optimization process, the targets were subjected to energy minimization utilizing the Swiss PDB Viewer® software package, employing the GROMOS96 force field method, and saved in PDB file format (Chowdhury et al., 2023).

2.5.3 Molecular docking

Molecular docking was conducted on the selected ligands with the *alpha*-amylase and *alpha*-glucosidase enzymes using PyRx® software. In the docking process, the target enzyme was uploaded and converted into macromolecules. Subsequently, the ligand was loaded and converted into the PDBQT format. We performed blind docking, setting the grid box to its maximum along the X, Y, and Z axes. The docking results of the study were saved in the CSV file format, and the best pose was extracted in the PDB file format. The interactions between the ligand and enzyme were visualized using Discovery Studio® software (Chowdhury et al., 2024). Additionally, non-bond interactions of the ligand and enzyme were visualized using Discovery Studio software (Chowdhury et al., 2024). Additionally, non-bond interactions of the ligand and enzyme were recorded.

2.6 Statistical analysis

The assays were performed in triplicates, and the obtained values are stated as mean ± SD. For the *in vitro* investigation of α-amylase and α-glucosidase inhibitory properties, the IC_{50} was obtained from the graph plots of the dose–response curves at each oil concentration via Graph Pad Prism® software (San Diego, CA, United States). The IC_{50} is the concentration of the extract required to inhibit 50% of the tested enzyme activity under the applied assay conditions.

3 Results and discussion

3.1 UPLC-ESI/MSⁿ metabolic profiling of the 80% methanol extracts of *C. odorata* and *T. ciliata*

The search for natural therapeutic agents is increasing nowadays due to their advantages of being safe, effective, and readily available. ThegGenus *Cedrela* is one of the well-known and understudied genera with many beneficial health activities, including cytotoxic (Choi et al., 2015), antiviral, hepatoprotective (leaves) (Asaad et al., 2021), anti-microbial (leaves) (Paritala et al., 2015), hypoglycemic (bark) (Giordani et al., 2015), antioxidant (bark) (Shah and Patel, 2021; Kumari and Kakkar, 2008), anti-leishmania (Takahashi et al., 2004), and anti-larval activities (Koul, 1983). The UPLC-ESI/MSⁿ technique was used to identify the phytoconstituents of the 80% methanol extracts of *Cedrela* species (*Cedrela odorata* and *Toona ciliata*). As shown in Figure 1 and Table 1, the UPLC-ESI/MSⁿ analysis resulted in the tentative identification of 55 compounds with their specific fragmentation patterns (% identification ranged from 88.61% to 89.38%). Different phytochemical classes were detected, including flavonoids, phenylpropanoids, terpenes, and tannins. The tentatively identified compounds can be summarized as follows. The fragmentation patterns of the identified compounds are illustrated in Supplementary Figures S1–S14.

3.1.1 Flavonoids

Twenty-two flavonoids were tentatively identified from the extracts of *Cedrela odorata* and *Toona ciliata* representing the major class of identified compounds (Table 1; Figure 2). A deprotonated molecular ion peak was shown at $[M-H]^-$ m/z 273 (R_t = 0.70 min, only in *C. odorata*) and was tentatively identified as afzelechin (Zaghloul et al., 2023). Another flavonoid peak was traced in the ESI negative ion mode at m/z 531 (R_t = 1.05 min, 4.33% *T. ciliata,* 8.00% *C. odorata*) with fragments at m/z 300, 388, 219, and 101 thus it was assigned to icariside I (Ren and Long, 2017). In addition to that, 16 different flavonoid glycosides were tentatively identified at different retention times and can be detailed as follows. A molecular ion peak was detected at $[M-H]^-$ m/z 431 and $[M + H]^+$ m/z 433 with one major fragment at m/z 285 due to loss of kaempferol aglycone and was tentatively identified as kaempferol-3-*O*-pentoside (Chen Q. et al., 2011). Another pentoside was detected at m/z 447 in the ESI negative ion mode and m/z 449 in the ESI positive ion mode with daughter peaks at m/z 372, 153, 301, 284, 271, 254, and 239, where the quercetin aglycone was clear at m/z 301; thus, it was defined as quercetin-3-*O*-pentoside (5.80% *T. ciliata*) (Cunja et al., 2014; Sobeh et al., 2016). Two acetyl glycosides were detected at m/z 505 and m/z 489 and were tentatively assigned to quercetin-*O*-acetyl-hexoside (MS/MS at m/z 345, 301, 293, 239, 161, and 103; 3.00%, *C. odorata*) and kaempferol acetyl-hexoside (MS/MS at m/z 337 and 285; 7.09%, *T. ciliata*), respectively (Elhawary et al., 2021; Kramberger et al., 2020).

A deprotonated peak was shown at m/z 463 in the ESI negative mode with fragments at m/z 357, 310, 301, 308, 271, and 255 and was found to be a quercetin derivative, namely, quercetin-*O*-hexoside (Simirgiotis et al., 2015). Similarly, another kaempferol derivative
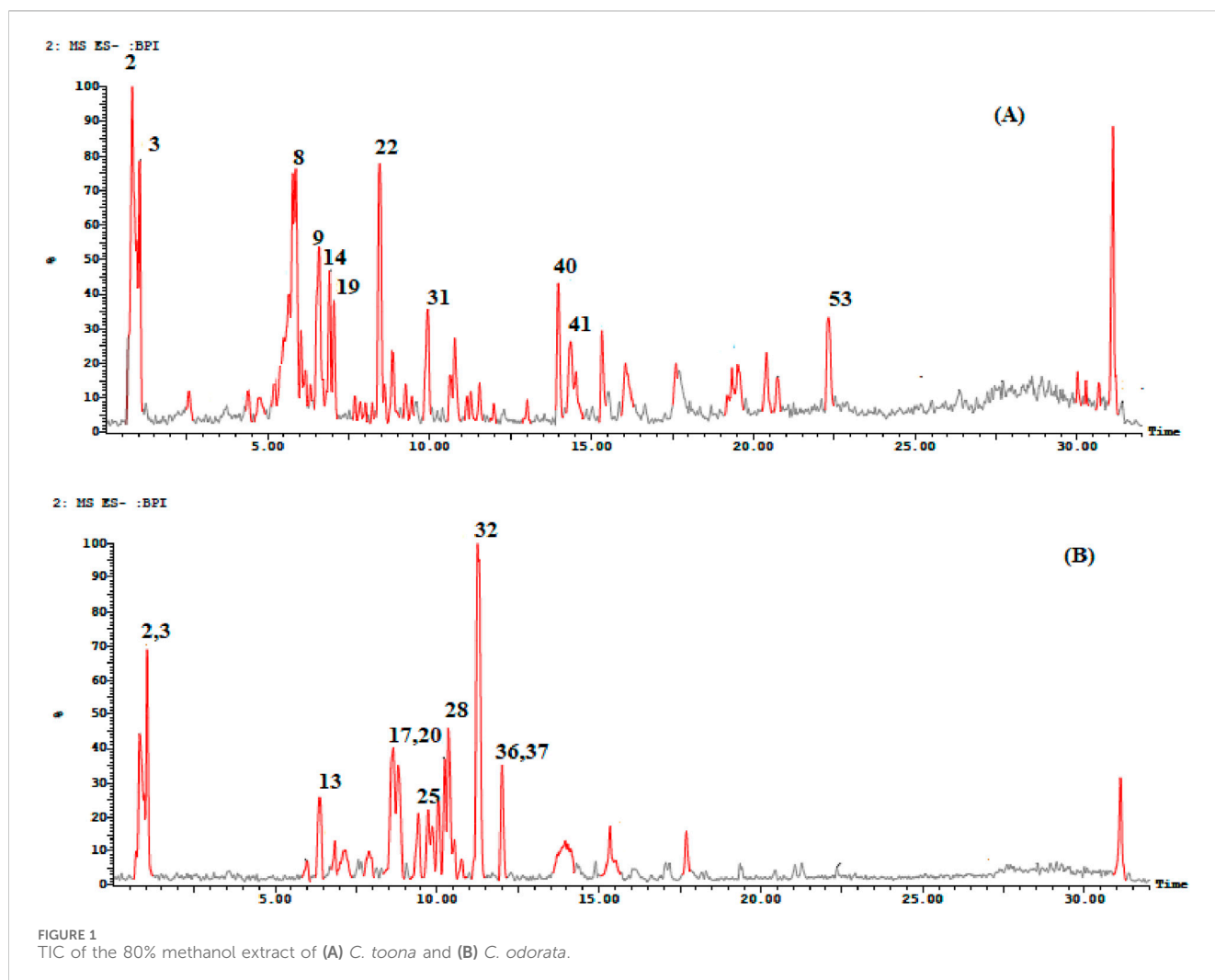
FIGURE 1
TIC of the 80% methanol extract of **(A)** *C. toona* and **(B)** *C. odorata*.

showed a molecular ion peak at [M-H]⁻ *m/z* 593 (5.12%, *C. odorata*) and was tentatively defined as kaempferol-deoxyhexosyl-hexoside (Elhawary et al., 2021). Compound 10 showed a deprotonated peak at *m/z* 609 in the ESI negative mode and was tentatively identified as rutin (Simirgiotis et al., 2015); it further showed one of its fragments at *m/z* 423 (Shrestha et al., 2017). In the same context, a peak was detected at [M-H]⁻ *m/z* 311 for the glycoside arbutin (Jia et al., 2017), together with its fragment at *m/z* 293 (Jia et al., 2017). Three compounds belonging to the flavonoid apigenin were detected at *m/z* 521 (9.60% *T. ciliata*) (Rini Vijayan and Raghu, 2019) and m/z 547 (Marzouk et al., 2019), both in the ESI negative ion mode for an apigenin derivative and apigenin 6-*C*-pentoside-8-*C*-pentoside, respectively, and their identity was confirmed by their fragmentation patterns detected as (*m/z* 285, 236, 196, 183, and 161) and (*m/z* 456, 425, 417, 285, 263, 237, and 135), respectively, where the kaempferol aglycone fragment was traced at *m/z* 285 in the two compounds. In addition, apigenin 6-*C*-α-pentoside-8-*C*-β-hexoside (isoviolanthin) was traced in the ESI positive ion mode at *m/z* 579 (Marzouk et al., 2019). Compound 6 presented a deprotonated peak at *m/z* 591 and MS/MS at *m/z* 289, 265, 255, 119, 133, and 103 and was tentatively assigned to the glycoside acacetin pento-hexoside (Al-Yousef et al., 2020).

Moreover, chrysoeriol-7-*O*-hexouronic acid showed its deprotonated peak at *m/z* 475 (El Sayed et al., 2016a). Compound 25 was tentatively defined as manniflavanone with a deprotonated peak at *m/z* 589 in the ESI negative ion mode and daughter peaks at *m/z* 443, 399, 341, 331, 306, 287, 265, 123, and 113 (7.06%, *C. odorata*) (Reed, 2009). Only one myricetin derivative was tentatively detected at [M-H]⁻ *m/z* 655 and was identified as myricetin-*O*-hexosyl-*O*-hexouronoside (MS/MS at *m/z* 285 and 179; 3.15%, *T. ciliata*) (Affes et al., 2021). Three different flavonoid glycosides were tentatively traced in the ESI positive ion mode at *m/z* 451, *m/z* 609, and *m/z* 623 and were assigned to eriodictyol-7-*O*-hexoside (Ashraf et al., 2020), rhamnocitrin-*O*-rutinoside (ElKhateeb et al., 2019), and isorhamnetin 7-*O*-[3-hydroxy-3- methylglutaroyl]-hexoside (López-Angulo et al., 2018), respectively.

3.1.2 Tannins

As shown in Table 1 and Figure 2, ten tannins and their fragments were identified from the two *Cedrela* extracts. A deprotonated peak was detected at *m/z* 471 in the ESI negative mode and was attributed to the compound, 3-methyl-epigallocatechin gallate (Bastos et al., 2007). Moreover, a fragment of (epi) gallocatechin was traced at *m/z* 467 (Escobar-Avello et al., 2019). In addition to that, two catechin-containing

TABLE 1 UPLC-ESI/MS^n metabolic profiling of the phytoconstituents of *T. ciliata* and *C. odorata* in the negative and positive ion modes.

No.	Compound	Molecular formula	Class	R_t (min.)	[M-H]$^-$ (m/z)	[M + H]$^+$/[M + H + Na]$^+$ (m/z)	MS/MS fragments	% composition		Ref.
								TC	CO	
1	Afzelechin	C$_{15}$H$_{14}$O$_5$	Flavonoid	0.70	273	—	—	—	1.81	Zaghloul et al. (2023)
2	Fragment	—	—	0.71	377	381	—	14.76	8.79	Benayad et al. (2014)
3	Icariside I	C$_{27}$H$_{30}$O$_{11}$	Flavonoid	1.05	531	—	300, 388, 219, and 101	4.33	8.00	Ren and Long (2017)
4	Chlorogenic acid derivative	—	Phenylpropanoid	2.57	451	—	298, 276, 191, 169, 108, and 71	0.51	—	Simirgiotis et al. (2015)
5	Kaempferol-*O*-pentoside	C$_{20}$H$_{18}$O$_{10}$	Flavonoid	4.39	431	433	285	2.87	3.52	Chen H. J et al. (2011)
6	Acacetin pento-hexoside	C$_{28}$H$_{32}$O$_{14}$	Flavonoid	4.77	591	—	289, 265, 255, 119, 133, and 103	0.87	—	Al-Yousef et al. (2020)
7	Fragment of (epi)gallocatechin	—	Tannin	5.21	467	—	409, 347, 289, 283, 255, 101, and 99	0.58	—	Escobar-Avello et al. (2019)
8	Fragment of ursolic acid	—	Triterpene	5.40	411	—	265, 247, 179, 163, and 119	11.03	—	Chen H. J et al. (2011)
9	Apigenin derivative	—	Flavonoid	5.87	521	—	285, 236, 196, 183, and 161	9.60	—	Rini Vijayan and Raghu (2019)
10	Rutin	C$_{27}$H$_{30}$O$_{16}$	Flavonoid	5.99	609	—	315, 301, 209, 188, and 83	—	1.97	Simirgiotis et al. (2015)
11	Quercetin-*O*-hexoside	C$_{21}$H$_{20}$O$_{12}$	Flavonoid	6.16	463	—	357, 310, 301, 308, 271, and 255	0.76	—	Simirgiotis et al. (2015)
12	Salvianolic acid A	C$_{26}$H$_{22}$O$_{10}$	Miscellaneous	6.32	493	—	403, 165, 133, 121, 101, and 99	0.25	—	Barros et al. (2013)
13	Kaempferol-deoxyhexosyl-hexoside	C$_{27}$H$_{29}$O$_{14}$	Flavonoid	6.38	593	—	285, 227, 209, and 169	—	5.12	Elhawary et al. (2021)
14	Quercetin-3-*O*-pentoside	C$_{20}$H$_{18}$O$_{11}$	Flavonoid	6.59	447	449	372, 153, 301, 284, 271, 254, and 239	5.80	—	Cunja et al. (2014), Sobeh et al. (2016)
15	Aloeresin B	C$_{19}$H$_{22}$O$_9$	Anthraquinone	6.70	393	—	307, 277, 163, and 113	0.37	—	El Sayed et al. (2016b)
16	Quinic acid derivative	—	Phenylpropanoid	6.81	441	—	265, 235, 191, 175, and 89	0.36	2.12	Chen Q et al. (2011)
17	Quercetin-*O*-acetyl-hexoside	C$_{23}$H$_{22}$O$_{13}$	Flavonoid	7.17	505	—	345, 301, 293, 239, 161, and 103	—	3.00	Elhawary et al. (2021)
18	3,5-di-*O*-Caffeoylquinic acid	C$_{25}$H$_{24}$O$_{12}$	Phenylpropanoid	7.69	515	—	321, 303, 271, 261, and 191	2.14	—	Chen Q et al. (2011)
19	Chicoric acid derivative	—	Phenylpropanoid	7.86	473	—	328, 266, 243, 209, and 101	3.33	—	Chen H. J et al. (2011)
20	Caffeic acid hexoside derivative	—	Phenylpropanoid	7.90	533	—	388, 371, 330, 319, 299, and 269	—	7.36	Elhawary et al. (2021)
21	3-Methyl-epigallocatechin gallate	C$_{23}$H$_{20}$O$_{11}$	Tannin	8.23	471	—	289 and 140	0.23	—	Bastos et al. (2007)
22	Kaempferol acetyl-hexoside	C$_{23}$H$_{22}$O$_{12}$	Flavonoid	8.46	489	—	337 and 285	7.09	—	Kramberger et al. (2020)
23	Chrysoeriol-*O*-hexouronic acid	C$_{22}$H$_{20}$O$_{12}$	Flavonoid	8.61	475	—	—	0.73	—	El Sayed et al. (2016a)
24	(epi)afzelechin–(epi)catechin dimer	C$_{30}$H$_{25}$O$_{11}$	Tannin	9.25	561	—	273	1.02	—	Gu et al. (2003)
25	Manniflavanone	C$_{30}$H$_{22}$O$_{13}$	Flavonoid	9.43	589	—	443, 399, 341, 331, 306, 287, 265, 123, and 113	—	7.06	Reed (2009)

(Continued on following page)

TABLE 1 (*Continued*) UPLC-ESI/MS^n metabolic profiling of the phytoconstituents of *T. ciliata* and *C. odorata* in the negative and positive ion modes.

No.	Compound	Molecular formula	Class	R_t (min.)	[M-H]$^-$ (m/z)	[M + H]$^+$/[M + H + Na]$^+$ (m/z)	MS/MS fragments	% composition		Ref.
								TC	CO	
26	Fragment of caffeoyl diferuloylquinic acid	—	Phenylpropanoid	9.56	—	545	—	0.53	—	Schmeda-Hirschmann et al. (2015)
27	13-*O*-Phenylacetyl-12- deoxyphorbol-20-acetate	C$_{30}$H$_{36}$O$_7$	Miscellaneous	10.25	531	—	265, 119, and 101	—	**5.20**	Ghani and Badr (2020)
28	Ganolucidic acid B	C$_{30}$H$_{46}$O$_6$	Triterpene	10.37	501	503	213	—	**7.24**	Yang et al. (2007)
29	(epi)Catechin-ethyl dimer	—	Tannin	10.64	605	—	289	1.14	—	Rockenbach et al. (2012)
30	Apigenin 6-*C*-pentoside-8-*C*-pentoside	C$_{25}$H$_{26}$O$_{13}$	Flavonoid	10.76	547	—	456, 425, 417, 285, 263, 237, and 135	—	2.03	Marzouk et al. (2019)
31	Pallidol	C$_{28}$H$_{22}$O$_6$	Stilbene dimer	10.78	453	—	364, 245, 240, and 111	2.64	—	Escobar-Avello et al. (2019)
32	Ferulic acid derivative	—	Phenylpropanoid	11.28	517	551	266, 255, 241, and 212	0.53	**13.79**	Bystrom et al. (2008)
33	Abscisic acid-*O*-hexoside-HMG	—	Tannin	11.54	585	—	—	0.76	—	El-Sayed et al. (2017)
34	7,8-Dihydro-3- oxo-α-ionol β-D-hexoside	C$_{13}$H$_{22}$O$_2$	Miscellaneous	11.88	—	373	—	—	1.11	El-sayed et al. (2021)
35	Arbutin	C$_{12}$H$_{16}$O$_7$	Flavonoid	11.98	311	—	—	0.36	—	Jia et al. (2017)
36	A-type proanthocyanidin dimer	C$_{30}$H$_{24}$O$_{12}$	Tannin	12.00	575	—	459, 443, 211, and 175	—	**5.65**	Reed (2009)
37	Secoisolariciresinol guaiacylglyceryl ether	C$_{30}$H$_{38}$O$_{10}$	Sesquilignan	12.25	—	559	403, 379, and 337	—	**4.38**	Patyra et al. (2022)
38	Procyanidin dimer	C$_{30}$H$_{26}$O$_{12}$	Tannin	13.01	573	—	—	0.51	—	Reed (2009)
39	Methyl trigalloyl hexose	C$_{28}$H$_{27}$O$_{18}$	Tannin	13.96	649	—	539, 529, 499, 455, and 359	—	**5.95**	El-sayed et al. (2021)
40	Eicosanoyl derivative of 12-ursen-3-ol	C$_{50}$H$_{88}$O$_2$	Triterpene	13.97	721	—	577, 411, and 289	2.79	—	Xiao et al. (2023)
41	Fragment of arbutin	—	Flavonoid	14.35	293	—	163, 113, and 89	2.33	—	Jia et al. (2017)
42	Heliarzanol 1	C$_{24}$H$_{30}$O$_8$	Pyrone derivative	16.06	445	—	206, 193, 164, and 112	2.22	—	Kramberger et al. (2020)
43	Apigenin 6-*C*-α-pentoside-8-*C*-β-hexoside (isoviolanthin)	C$_{27}$H$_{30}$O$_{14}$	Flavonoid	16.52	—	579	374, 259, and 199	1.42	1.15	Marzouk et al. (2019)
44	Chlorogenic acid	C$_{16}$H$_{18}$O$_9$	Phenylpropanoid	17.91	—	353	299, 251, and 209	0.47	1.38	Elhawary et al. (2021)
45	Fragment of rutin	—	Flavonoid	19.20	423	—	379, 327, and 294	**3.16**	—	Shrestha et al. (2017)
46	Eriodictyol-7-*O*-hexoside	C$_{21}$H$_{22}$O$_{11}$	Flavonoid	19.38	—	451	264, 203, and 169	—	0.78	Ashraf et al. (2020)
47	Caffeoyl-2-hydroxyethane-1,1,2-tricarboxylic acid	—	Phenylpropanoid	20.40	339	—	265, 179, and 103	1.68	—	Ye et al. (2005), Ben Said et al. (2017)
48	Fragment of chlorogenic acid	—	Phenylpropanoid	20.73	313	—	—	0.98	—	Ibrahim et al. (2015)
49	Acetyl-*O*-galloyl hexose	C$_{14}$H$_{19}$O$_{10}$	Tannin	20.82	—	375	—	0.60	—	El-sayed et al. (2021)
50	Rhamnocitrin-*O*-rutinoside	—	Flavonoid	20.96	—	609	315, 209, and 188	1.94	—	ElKhateeb et al. (2019)

TABLE 1 *(Continued)* UPLC-ESI/MS^n metabolic profiling of the phytoconstituents of *T. ciliata* and *C. odorata* in the negative and positive ion modes.

No.	Compound	Molecular formula	Class	R_t (min.)	[M-H]$^-$ (m/z)	[M + H]$^+$/[M + H + Na]$^+$ (m/z)	MS/MS fragments	% composition TC	% composition CO	Ref.
51	Trigalloyllevohexosan	–	Tannin	21.13	–	621	509, 445, and 223	–	0.62	El-sayed et al. (2021)
52	Myricetin-O-hexosyl-O-hexouronoside	–	Flavonoid	22.32	655	–	285 and 179	3.15	–	Affes et al. (2021)
53	Isorhamnetin 7-O-[3-hydroxy-3- methylglutaroyl]-hexoside	–	Flavonoid	22.87	–	623	315, 270, 168, and 75	11.07	6.57	López-Angulo et al. (2018)
54	Galloyl ester of 5,6,7- trihydroxy-2,3- dihydrocyclopenta [b] chrom ene-1,9-dione-3-carboxylic acid hexoside	–	Miscellaneous	24.07	–	607	547 and 460	20.98	17.28	Fraternale et al. (2015)
55	12-O-β-D-hexoside deriv. of 8,11,13-Abietatriene-3,11,12,16-tetrol	$C_{26}H_{40}O_9$	Diterpene	30.01	597	–	–	0.50	–	Lee et al. (2016)
	% Identification ESI –ve mode ESI + ve mode							89.38 37.00	88.61 33.27	

Bold font indicates high percentage of compounds.

dimers were tentatively identified as compounds 24 and 29. The former showed its peak at [M-H]$^-$ *m/z* 561 and was assigned to (epi) afzelechin–(epi) catechin dimer (Gu et al., 2003), while the latter had a peak at [M-H]$^-$ *m/z* 605 and was defined to be (epi) catechin-ethyl dimer (Rockenbach et al., 2012).

Compound 33 with a deprotonated peak at the *m/z* 585 in negative mode was identified as abscisic acid-*O*-hexoside-HMG (El-Sayed et al., 2017). On the other hand, compounds 36 and 38 showed deprotonated peaks at *m/z* 575 (5.65% *C. odorata*) and *m/z* 573 in the ESI negative mode (MS/MS at *m/z* 459, 443, 211 and 175) and were identified as A-type proanthocyanidin dimer and procyanidin dimer, respectively (Reed, 2009). Regarding the hydrolysable tannins, three of them were traced at *m/z* 649 (ESI negative), m/z 375 (ESI positive), and m/z 621 (ESI positive) and were tentatively assigned to methyl trigalloyl hexose (5.95% *C. odorata*), acetyl-*O*-galloyl hexose, and trigalloyl hexose, respectively (El-sayed et al., 2021).

3.1.3 Phenylpropanoids

Ten phenylpropanoids were traced (Table 1; Figure 2) and can be detailed here; compound 16 showed a deprotonated peak at [M-H]$^-$ *m/z* 441 and was identified as a quinic acid derivative (Chen H. J. et al., 2011). Similarly, compound 18 was also a quinic acid-containing phenylpropanoid with a parent peak at *m/z* 515 in the ESI negative mode and was defined as 3,5-di-*O*-caffeoylquinic acid (Chen H. J. et al., 2011). A fragment of caffeoyl diferuloylquinic acid was detected at [M + H]$^+$ *m/z* 545 (Schmeda-Hirschmann et al., 2015). Moreover, another parent peak was traced at *m/z* 533 with its fragments at *m/z* 388, 371, 330, 319, 299, and 269 (ESI negative, 7.36% *C. odorata*) and was attributed to the presence of a caffeic acid hexoside derivative (Elhawary et al., 2021). Compounds 4,44 and 48 were showing parent peaks at *m/z* 451 (ESI–ve), *m/z* 353 (ESI + ve), and *m/z* 313 (ESI–ve) and were tentatively identified as a chlorogenic acid derivative (Simirgiotis et al., 2015), chlorogenic acid (Elhawary et al., 2021), and a fragment of chlorogenic acid (Ibrahim et al., 2015), respectively. The aforementioned compounds shared the presence of one characteristic fragment at *m/z* 191 due to the quinic acid fragment. A deprotonated molecular ion peak was detected at [M-H]$^-$ *m/z* 473 with MS/MS at *m/z* 328, 266, 243, 209, and 101 (3.33% *T. ciliata*) and was identified as a chicoric acid derivative (Chen H. J. et al., 2011). Compound 32 showed a parent peak at [M-H]$^-$ *m/z* 517 and [M + H + CH$_3$O]$^+$ *m/z* 551 (MS/MS at *m/z* 266, 255, 241, and 212) and was assigned to a ferulic acid derivative (13.79% *C. odorata*) (Bystrom et al., 2008). Another phenylpropanoid peak was detected at the *m/z* 339 in ESI negative mode and was tentatively found to be caffeoyl-2-hydroxyethane-1,1,2-tricarboxylic acid (Ye et al., 2005; Ben Said et al., 2017).

3.1.4 Triterpenes

Two triterpenes were detected (Table 1; Figure 2). The first one presented a parent peak at *m/z* 501 in the ESI negative mode and *m/z* 503 in the ESI positive mode with one fragment at *m/z* 213 (7.24% *C. odorata*), and it was defined as the triterpene, ganolucidic acid B (Yang et al., 2007). The second triterpene peak was shown at *m/z* 721 in the ESI negative mode and was tentatively assigned to the eicosanoyl derivative of 12-ursen-3-ol (Xiao et al., 2023).
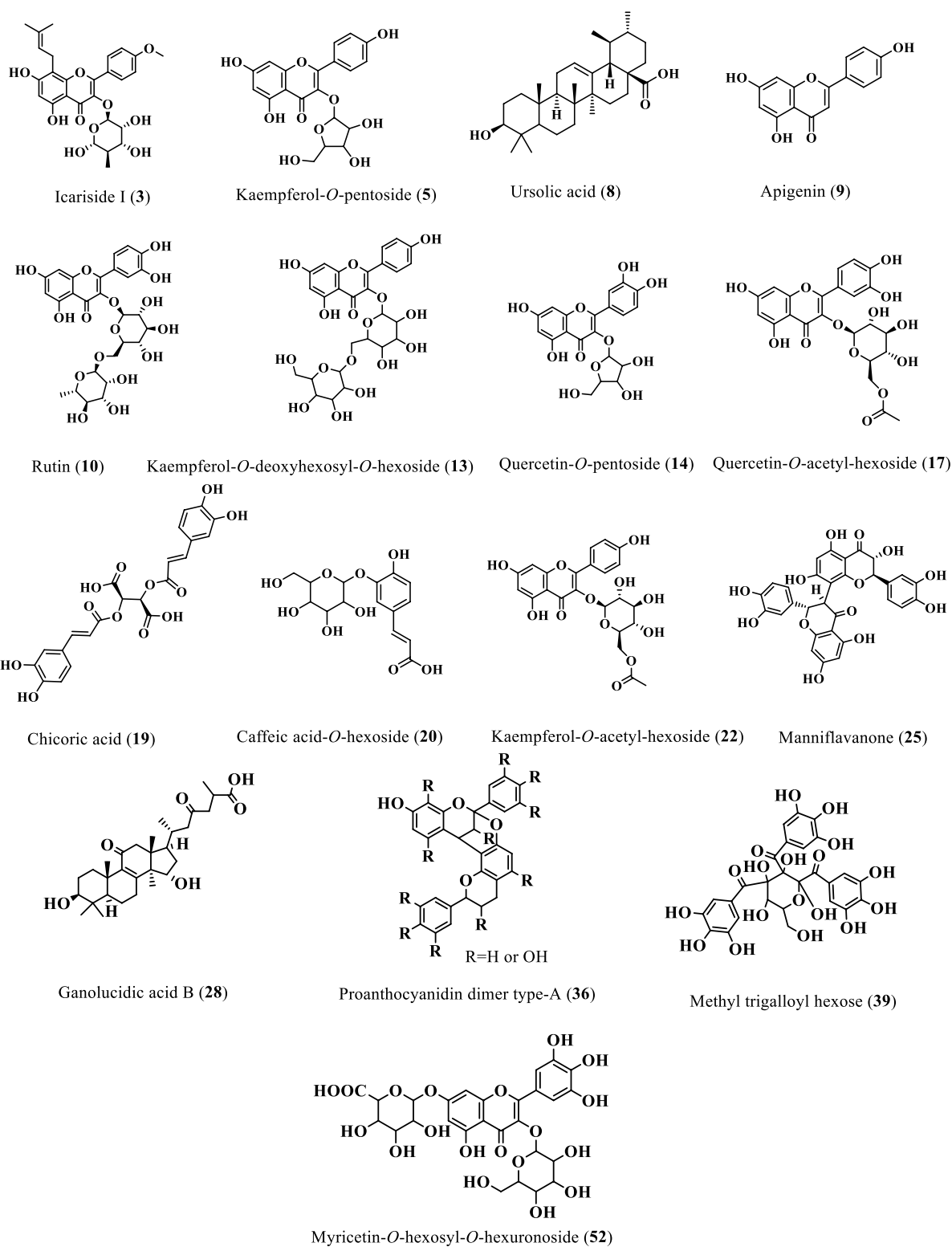
FIGURE 2
Structures of the major identified phytoconstituents of the 80% methanol extracts of *T. ciliata* and *C. odorata*.

3.1.5 Diterpenes

Only one diterpene derivative was traced from the *T. ciliata* extract (Table 1; Figure 2). This diterpene was identified as 12-*O*-β-D-hexoside derivative of 8,11,13-abietatriene-3,11,12,16-tetrol, and it showed a deprotonated peak at [M-H]⁻ *m/z* 597 (Lee et al., 2016).

Herein, 55 phytoconstituents were tentatively identified and quantified from two species of *Cedrela,* namely, *C. odorata* and

TABLE 2 α-Amylase and α-glucosidase inhibitory activities of 80% methanol leaf extracts of *C. odorata* and *T. ciliata*, compared to standard drugs.

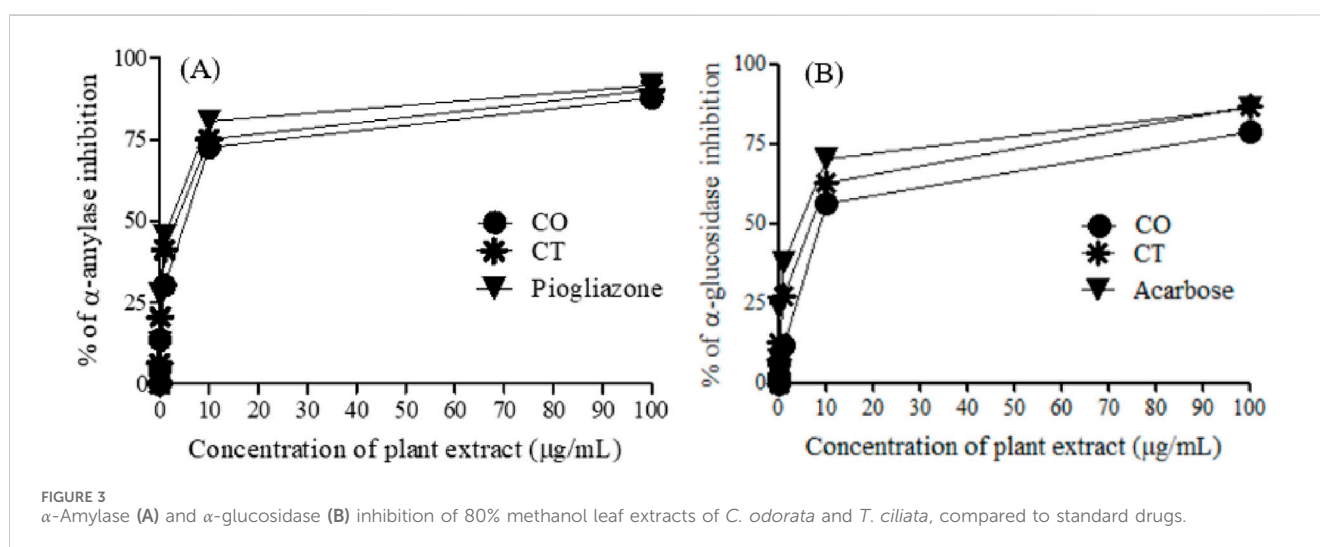| Concentration (μg/mL)	α-Amylase inhibition (%)			α-Glucosidase inhibition (%)		
	CO	CT	Pioglitazone	CO	CT	Acarbose
0.01	4.45 ± 1.56	6.29 ± 1.60	12.50 ± 2.05	2.08 ± 2.63	7.46 ± 1.70	7.41 ± 1.23
0.10	13.50 ± 2.60	20.50 ± 2.35	27.70 ± 1.28	6.44 ± 1.95	12.80 ± 2.02	23.60 ± 2.01
1.00	30.20 ± 1.29	41.20 ± 1.73	45.40 ± 2.45	11.80 ± 1.29	27.40 ± 1.63	37.60 ± 0.42
10.00	72.60 ± 2.22	75.10 ± 1.96	80.60 ± 0.23	56.30 ± 2.56	62.90 ± 0.58	70.20 ± 1.28
100.00	87.90 ± 1.67	90.30 ± 2.08	91.70 ± 1.05	78.60 ± 1.89	86.60 ± 1.87	86.10 ± 0.75
IC$_{50}$ (μg/mL)	4.83 ± 0.01	3.50 ± 0.03	2.17 ± 0.23	7.17 ± 0.01	6.50 ± 0.69	4.83 ± 1.02

*Values represent means ± SD (standard deviations) for triplicate experiments.

FIGURE 3
α-Amylase **(A)** and α-glucosidase **(B)** inhibition of 80% methanol leaf extracts of *C. odorata* and *T. ciliata*, compared to standard drugs.

T. ciliata. This study represents the first study with in-depth phytochemical profiling of two understudied *Cedrela* species through UPLC/MS analysis in both positive and negative ion modes, accompanied with identification and quantification of their metabolites with fragmentation patterns and comparison to the available literature.

Upon reviewing the LC/MS literature on genus *Cedrela*, few reports were found on these two species in particular. Bark and heartwood extracts of *T. ciliata* showed the presence of toonacillin, 6-hydroxy-toonacillin, and geranyl geraniol as its fatty esters (Shah and Patel, 2021). Limonoids (triterpenes), proanthocyanidins, flavonoids, and phenols were evaluated from 70 samples of *C. odorata* leaves through HPLC-UV-DAD, and it was found that the main identified components were kaempferol glycoside and catechin, while β-elemene, E-caryophyllene, aromadendrene, α-humulene, γ-cadinene, D-germacrene, bicyclogermacrene, α-tocopherol, and β-sitosterol were the main detected compounds using GC/MS analysis for the same samples (Bellone et al., 2021). In addition to that, other relevant members of the family Meliaceae were evaluated using LCMS analysis, and a study on *Melia azedarach* L. was performed utilizing UPLC/MS/MS analysis where 29 components were identified, including flavonoid *O*-glycosides, simple flavonoids, triterpenoid saponins, and

cardenolides as the major constituents (Saeed et al., 2022). Moreover, *Azadirachta indica* (the neem plant) leaf extract was analyzed through UPLC/MS where limonoids were revealed as the major contributing components of its metabolic profile (Rangiah et al., 2016).

Four triterpenes were isolated from *C. odorata* wood ethanol extract including gedunin, 3β-O-β-D-glucopyranosyl-24-methyllenecholesterol, oleanolic acid, sitosterol, n-octacosanol, and threo-23,24,25-trihydroxytirucall-7-en-3-one (Campos et al., 1991). In addition to that, calamenene, cycloeucalenol, sitosterol, stigmasterol, campesterol, gedunin, 7-deacetylgedunin, 7-deacetoxy-7-oxogedunin, methylangolensate, febrifugin, azadiradione, 20,21,22,23-tetrahydro-23-oxoazadirone, 3β-deacetylfissinolide and catechin, 1 α-methoxy-1,2-dihydrogedunin, and 3β-O-β-D-glucopyranosylcycloeucalenol were isolated from the stem extract of *C. odorata* (de Paula et al., 1997).

7-deoxo-7α,11β-diacetoxykihadanin A; 1,2-dihydro-7-deoxo-1α,7α,11β-triacetoxykihadanin A; cedrelosin F, 11β-acetoxylimonol; and 11β-acetoxycedrelosin B were defined from the stem bark extract of *C. odorata* (Bellone et al., 2021). Similarly, 4,5-dihydroblumenol A, 7-megastigmene-3α,6,9-triol, catechin, scopoletin, homovanillic alcohol, and 2-(3,4-dimethoxyphenyl)-

TABLE 3 Molecular docking affinity scores among the selected ligands with α-amylase and α-glucosidase enzymes.

Ligand	Molecular docking affinity (kcal/mol)	
	α-Amylase (4GQR)	α-Glucosidase (3TOP)
Apigenin	−8.2	−9.1
Caffeic acid hexoside	−7.9	−7.5
Chicoric acid	−8.6	−8.8
Ganolucidic acid B	−8.4	−8.4
Icariside I	−7.9	−8.4
Kaempferol acetyl-hexoside	−7.7	−9.1
Kaempferol-3-O-pentoside	−7.6	−9.2
Kaempferol-deoxyhexosyl-hexoside	−9.0	−8.7
Manniflavanone	−8.8	−9.2
Methyl trigalloyl hexose	−8.8	−9.5
Myricetin-O-hexosyl-O-hexuronoside	−9.1	−9.4
Quercetin-3-O-pentoside	−7.8	−8.8
Quercetin-O-acetyl-hexoside	−8.1	−9.3
Rutin	−9.3	−9.6
Ursolic acid	−9.4	−8.6
Acarbose	-	−7.6
Pioglitazone	−7.9	-

TABLE 4 Best top three ligand interactions with the alpha-amylase enzyme based on the binding affinity.

Ligand	Target	No. of HBs	HB residues	HB distance (Å)	Other bond residues
Myricetin-O-hexosyl-O-hexuronoside	α-amylase (4GQR)	09	HIS A:491 ASP A:456 GLN A:7 ARG A:10 LYS A:35 ARG A:392 ARG A:424 GLN A:8 GLY A:36	2.30 2.18 2.25 2.93 2.30 2.87 2.53 3.24 3.20	ILE A:396, VAL A:400
Rutin		06	ASP A:402 ARG A:10 SER A:289 GLN A:8 ARG A:421 THR A:11	2.95 2.97 2.84 2.28 2.76 3.32	PRO A:332
Ursolic acid		01	GLU A:233	2.54	LEU A:162, ALA A:198, TRP A:58, TRP A:59, TYR A:62, HIS A:305
Pioglitazone		02	ASP A:356 TRP A:59	2.00 2.41	HIS A:305, TRP A:59

HB, hydrogen bond.

ethyl-O-β-D-glucopyranoside were isolated from the stem bark of *C. odorata* (Muñoz Camero et al., 2018). Through HPLC, cedrodorin, 6-acetoxycedrodorin, 6-deoxy-9α-hydroxycedrodorin, and 9α-hydroxycedrodorin were isolated from the leaves of *C. odorata* (Veitch et al., 1999). Moreover, methylangolensate was detected from the heartwood of *C. odorata* (Chan et al., 1967). From the extracts of the leaves and twigs of *C. odorata*, cedrodorols A and B were detected (Wu et al., 2014). A triterpenoid, belonging to the limonoids, called odoratin was isolated from *C. odorata* (Chan et al., 1966).

Myricetin-*O*-hexosyl-*O*-hexuronoside/α-amylase complex

Rutin/α-amylase complex
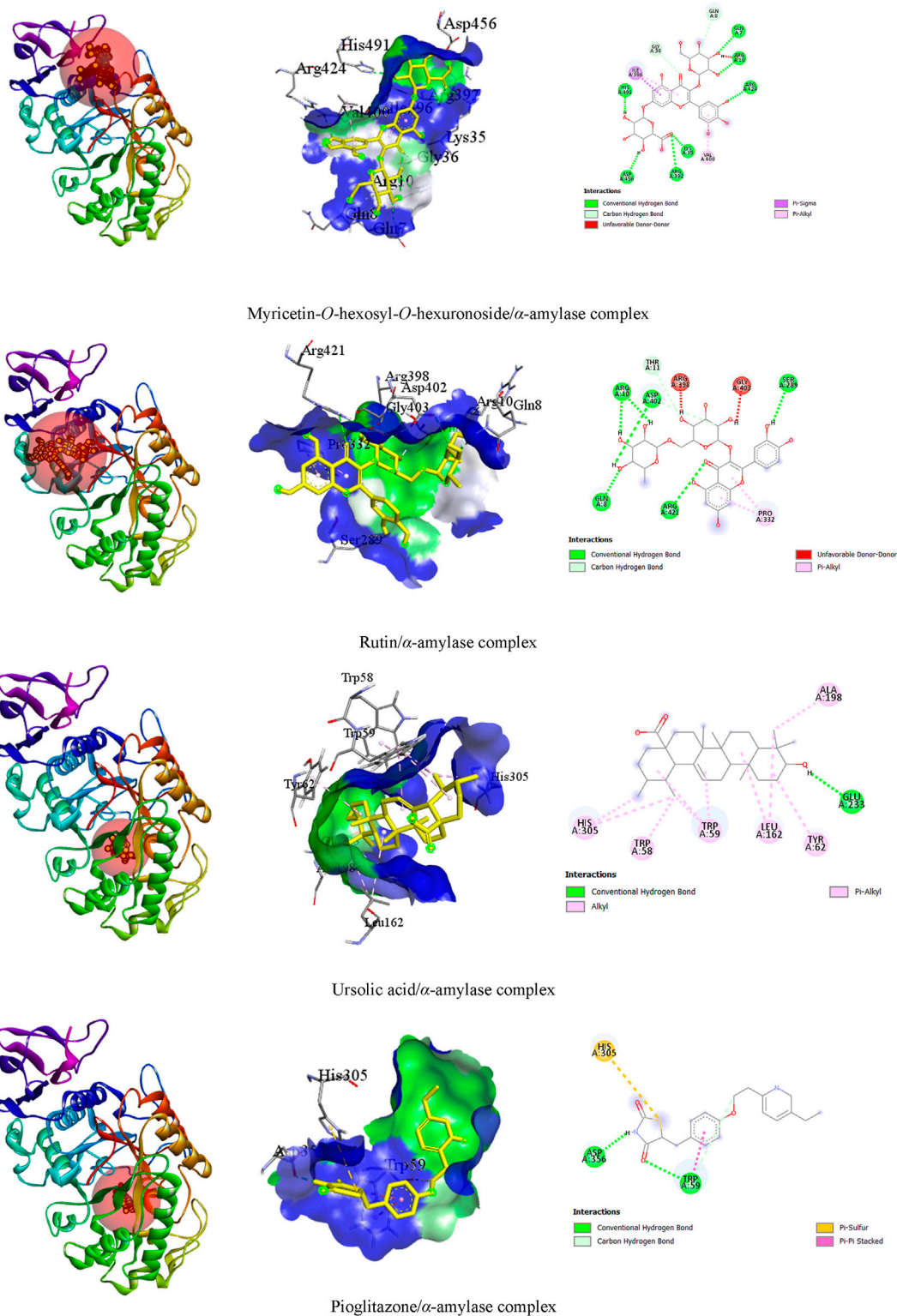
Ursolic acid/α-amylase complex

Pioglitazone/α-amylase complex

FIGURE 4
The 3D and 2D views of the top three ligand interactions with the α-amylase enzyme in the binding site highlight non-bond interactions.

TABLE 5 Best top three ligand interactions with the α-glucosidase enzyme (based on the binding affinity).

Ligand	Target	No. of HBs	HB residues	HB distance	Other bond residues
Methyl trigalloyl hexose	α-glucosidase (3TOP)	06	GLU A:1400 LEU A:1291 ALA A:1330 ASN A:1404 THR A:1290 LEU A:1401	2.48 2.42 2.40 2.17 3.62 2.87	PRO A:1329, LEU A:1291, ARG A:1410
Myricetin-O-hexoside-O-hexuronoside		04	TRP A:1355 ASP A:1157 TYR A:1251 GLN A:1286	2.46 2.37 1.93 2.77	TRP A:1355, ILE A:1587
Rutin		05	GLU A:1324 LEU A:1291 GLU A:1400 ARG A:1333 GLU A:1284	2.25 2.77 2.40 2.65 3.11	PRO A:1329
Acarbose		06	ASP A:965 TYR A:967 GLY A:992 ARG A:1453 ASP A:1454 HIS A:1449	2.53 2.53 2.22 1.98 2.35 3.57	—

HB, hydrogen bond.

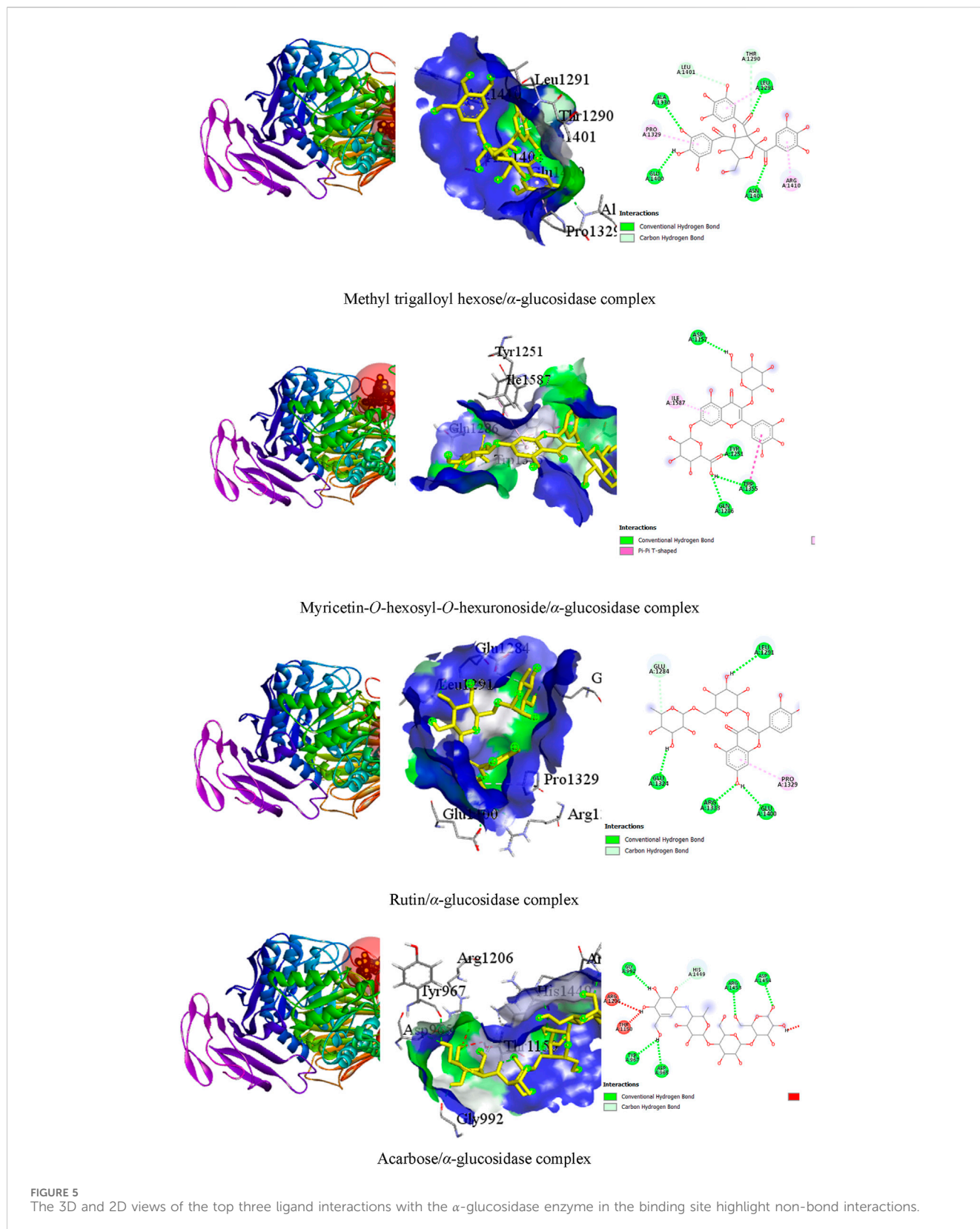## 3.2 Assessment of *in vitro* anti-diabetic activity

One of the therapeutic strategies for DM management is to retard hyperglycemia post-ingestion which can be achieved by inhibiting enzymes relevant to carbohydrate digestion like α-amylase and α-glucosidase (Ali et al., 2006). Thus, α-amylase and α-glycosidase enzyme inhibition assays were used to test *in vitro* anti-diabetic activities of the leaf extracts of *C. odorata* and *T. ciliata* (0.01, 0.10, 1.10, and 100 µg/mL), as shown in Table 2 and Figure 3.

The tested extracts and standard anti-diabetic drugs (pioglitazone and acarbose) showed concentration-dependent inhibition of α-amylase and α-glucosidase enzymatic activities. The leaf extracts of *C. odorata* and *T. ciliata* markedly inhibited α-amylase activities with IC$_{50}$ values of 4.83 ± 0.01 and 3.50 ± 0.03 µg/mL, respectively, compared to standard pioglitazone (standard α-amylase inhibitor; 2.17 ± 0.23 µg/mL). Furthermore, they showed significant α-glycosidase inhibitory properties with IC$_{50}$ values of 7.17 ± 0.01 and 6.50 ± 0.69 µg/mL, respectively, compared to acarbose (α-glycosidase inhibitor; IC$_{50}$ = 4.83 ± 1.02 µg/mL). In this study, the leaf extract of *T. ciliata* demonstrated larger inhibition values of 90.30% ± 2.08% and 86.60% ± 1.87% for α-amylase and α-glucosidase, respectively, than those of *C. odorata* (87.90% ± 1.67% and 78.60% ± 1.89%) at concentration of 100 µg/mL. The results suggest the anti-diabetic potential of the tested extracts. Based on inhibiting the activities of these enzymes, they could delay carbohydrate digestion and prolong the overall time for carbohydrate digestion, resulting in a reduction in the rate of glucose absorption and consequently blunting the postprandial blood glucose rises, i.e., making food have lower glycemic index (Ahmad et al., 2012). Furthermore, the extract of *C. odorata* showed superior activity than that of *T. ciliata*; it may be attributed to the high percentage of flavonoids in *C. odorata* which acts synergistically to inhibit the activities of these metabolizing enzymes.

With the same line of our study, previous research reported that the hydroethanolic extract of *C. odorata* could blunt the postprandial glycemic surge in the streptozotocin-induced diabetic rat model (Giordani et al., 2015). According to our results, the reported anti-hyperglycemic activity was attributed to the inhibition of α-amylase and α-glucosidase activities. Thus, the anti-diabetic efficacy of Cedrela extracts could be due to the existence of active constituents with diverse mode of actions at the molecular level, comprising α-amylase and α-glycosidases.

Ursolic acid (**8**) as one of the major identified compounds (Figure 2) displays a positive effect on reducing blood glucose levels and alleviating the diabetes-related complications in several diabetic animal models such as streptozotocin-nicotinamide-induced diabetic mice (Lee et al., 2010), streptozotocin-induced diabetic mice fed a high-fat diet (Jang et al., 2009), and streptozotocin-induced diabetic mice (Jang et al., 2010). In the same manner, icariside I (**3**), was previously obtained from *Herba Epimedii* (Berberidaceae) and enhanced the type-2 diabetes mellitus profile in db/db mice in a dose-dependent manner (Li et al., 2022). Furthermore, the leaf extract of *Simarouba glauca* (Simaroubaceae) was reported to be rich in kaempferol-O-pentoside (**5**) and effectively inhibited α-glucosidase activities with IC$_{50}$ value of 2.4 0.4 µg/mL (Mugaranja and Kulal, 2020). Rutin (**10**) was found to reduce the carbohydrate absorption from the small intestine and inhibit tissue gluconeogenesis, along with glucose uptake activation (Ghorbani, 2017). Furthermore, it was reported to enhance insulin release from beta cells and protect Langerhans islet from degeneration via antioxidant activity (Jadhav and Puchchakayala, 2012).

Methyl trigalloyl hexose/α-glucosidase complex

Myricetin-*O*-hexosyl-*O*-hexuronoside/α-glucosidase complex

Rutin/α-glucosidase complex

Acarbose/α-glucosidase complex

FIGURE 5
The 3D and 2D views of the top three ligand interactions with the α-glucosidase enzyme in the binding site highlight non-bond interactions.

The quercetin aglycone was predominately identified in some compounds like **11**, **14**, and **17,** as shown in Table 1. A certain study reported that quercetin markedly inhibited α-amylase and α-glucosidase activities (Shen et al., 2023). Moreover, a combination of quercetin and rutin (**10**) displayed higher synergistic inhibition against these enzymes than the individual compounds (Oboh et al., 2015).

A combination of kaempferol (found in **5**, **13** and **22**) and myricetin (found in **52**) showed synergistic anti-diabetic activity in STZ-activated diabetes in rats via antioxidant and anti-inflammatory activities (Al-Abbasi and Kazmi, 2023).

Caffeic acid (found in **18**, **20**, **26**, and **47**) was reported to exhibit anti-hyperglycemic properties in C57BL/KsJ-*db/db* mice via enhanced glucokinase activity and glycogen content and concurrently depressed glucose-6-phosphatase and phosphoenolpyruvate carboxykinase activities accompanied by decreased glucose transporter-2 expression in the liver (Jung et al., 2006).

3.3 Molecular docking studies

3.3.1 Determination of affinity scores of the identified major components with α-amylase and α-glucosidase

Molecular docking, a computational technique, is utilized to position computer-generated 3D structures of small ligands within a receptor structure in various orientations, conformations, and positions. These ligands interact with the receptor through binding energy, providing insights into their pharmacological actions. In our docking simulation, the test ligands myricetin-*O*-hexosyl-*O*-hexuronoside, rutin, and ursolic acid exhibited the top three higher binding affinities with docking scores of −9.1, −9.3, and −9.4 kcal/mol, respectively, toward the *alpha*-amylase enzyme. Conversely, the standard ligand pioglitazone showed a binding affinity of −7.9 kcal/mol with the *alpha*-amylase enzyme. On the other hand, the test ligands methyl trigalloyl hexose, myricetin-*O*-hexosyl-*O*-hexuronoside, and rutin revealed the top three higher binding affinities with docking scores of −9.5, −9.4, and −9.6 kcal/mol, respectively, toward the *alpha*-glucosidase enzyme. In contrast, the standard ligand acarbose showed a binding affinity of −7.6 kcal/mol with the *alpha*-glucosidase enzyme. The binding affinities of other ligands with *alpha*-amylase and *alpha*-glucosidase enzymes are shown in Table 3.

3.3.2 Prediction of the active site of enzyme−ligand interactions

3.3.2.1 Top three test ligands and pioglitazone with α-amylase enzyme interactions

In our visualization of enzyme–ligand interactions, we observed that the test ligands myricetin-*O*-hexosyl-*O*-hexuronoside, rutin, and ursolic acid formed numerous hydrogen bonds and other bonds with amino acids in the α-amylase enzyme's binding pocket. Specifically, myricetin-*O*-hexosyl-*O*-hexuronoside created nine hydrogen bonds with HIS A:491, ASP A:456, GLN A:7, ARG A:10, LYS A:35, ARG A:392, ARG A:424, GLN A:8, and GLY A:36 amino acids, along with forming other bonds with ILE A:396 and VAL A:400 amino acids. Similarly, rutin formed six hydrogen bonds with ASP A:402, ARG A:10, SER A:289, GLN A:8, ARG A:421, and THR A:11 amino acids. Additionally, rutin established a hydrophobic bond with the PRO A:332 amino acid in the enzyme's binding site. Furthermore, ursolic acid showed one hydrogen bond with GLU A:233 amino acid and exhibited several hydrophobic bonds with LEU A:162, ALA A:198, TRP A:58, TRP A:59, and TYR A:62, as well as HIS A:305 amino acid. In contrast, pioglitazone interacted with the *alpha*-amylase enzyme by

forming two hydrogen bonds with ASP A:356 and TRP A:59 amino acid residues. Additionally, pioglitazone formed other bonding interactions with HIS A:305 and TRP A:59 amino acids (Table 4). The 3D and 2D views of the top three ligand interactions with the α-amylase enzyme in the binding site, highlighting non-bond interactions, are presented in Figure 4.

3.3.3 Top three test ligands and acarbose with α-glucosidase enzyme interactions

It was observed that the test ligands methyl trigalloyl hexose, myricetin-*O*-hexosyl-*O*-hexuronoside, and rutin formed numerous hydrogen bonds and other bonds with amino acids in the *alpha*-glucosidase enzyme's binding pocket. Specifically, methyl trigalloyl hexose created six hydrogen bonds with GLU A:1400, LEU A:1291, ALA A:1330, ASN A:1404, THR A:1290, and LEU A:1401 amino acids, along with forming other bonds with PRO A:1329, LEU A:1291, and ARG A:1410 amino acids. Similarly, myricetin-*O*-hexosyl-*O*-hexuronoside formed four hydrogen bonds with TRP A:1355, ASP A:1157, TYR A:1251, and GLN A:1286 amino acids. Additionally, rutin established hydrophobic bonds with TRP A:1355 and ILE A:1587 amino acids in the enzyme's binding site. Furthermore, rutin showed five hydrogen bonds with GLU A:1324, LEU A:1291, GLU A:1400, ARG A:1333, and GLU A:1284 amino acids and exhibited a hydrophobic bond with the PRO A:1329 amino acid. In contrast, acarbose interacted with the *alpha*-glucosidase enzyme by forming only six hydrogen bonds with ASP A:965, TYR A:967, GLY A:992, ARG A:1453, ASP A:1454, and HIS A:1449 amino acid residues (Table 5). The 3D and 2D views illustrating the top three ligand interactions with the *alpha*-glucosidase enzyme in the binding site, highlighting non-bond interactions, are presented in Figure 5.

4 Conclusion

This study presents the first report on the inhibitory ability of leaf extracts of *T. ciliata* and *C. odorata* against α-amylase and α-glucosidase. Likewise, this research showed a remarkable association between the major identified components of *Cedrela* extracts and α-amylase and α-glucosidase activity inhibition. The *in silico* molecular docking studies exhibited favorable high binding affinities of the components of *Cedrela* extracts like myricetin-*O*-hexosyl-*O*-hexuronoside, rutin, and ursolic acid with α-amylase and α-glucosidase. This speculated that these phytoconstituents may significantly contribute to enzyme inhibition activities. Knowing that it is difficult to categorize a single compound responsible for the whole inhibitory activity against these enzymes, we can predict, based on the experimental and *in silico* results, that the α-amylase and α-glucosidase inhibitory activities of plant extracts are a result of the synergistic outcome of these phytoconstituents, suggesting their anti-diabetic potential. However, our study was restricted to *in vitro* biological investigation of the plant extracts; therefore, the bioavailability assessment and toxicological profile have not been explored. In future studies, these aspects will also be assessed. In addition, additional studies are required for the isolation and identification of individual phytocomponents and assessing their anti-hyperglycemic effect.

Data availability statement

Author contributions

HE-N: conceptualization, investigation, project administration, and writing–original draft. AA-Q: data curation and writing–original draft. MB: software and writing–original draft. RC: methodology and writing–original draft. MA-M: resources and writing–review and editing. HE: visualization and writing–review and editing. AM: supervision and writing–review and editing. MT: supervision and writing–review and editing. MA: validation and writing–review and editing. EE: software and writing–original draft.

Funding

Conflict of interest

The authors declare that the research was conducted in the absence of any commercial or financial relationships that could be construed as a potential conflict of interest.

Publisher's note

All claims expressed in this article are solely those of the authors and do not necessarily represent those of their affiliated organizations, or those of the publisher, the editors, and the reviewers. Any product that may be evaluated in this article, or claim that may be made by its manufacturer, is not guaranteed or endorsed by the publisher.

Supplementary material

The Supplementary Material for this article can be found online at: https://www.frontiersin.org/articles/10.3389/fchem.2024.1462309/full#supplementary-material

References

Abdelghffar, E. A., El-Nashar, H. A., Fayez, S., Obaid, W. A., and Eldahshan, O. A. (2022). Ameliorative effect of oregano (*Origanum vulgare*) versus silymarin in experimentally induced hepatic encephalopathy. *Sci. Rep.* 12, 17854. doi:10.1038/s41598-022-20412-3

Affes, S., Ben Younes, A., Frikha, D., Allouche, N., Treilhou, M., Tene, N., et al. (2021). ESI-MS/MS analysis of phenolic compounds from *Aeonium arboreum* leaf extracts and evaluation of their antioxidant and antimicrobial activities. *Molecules* 26, 4338. doi:10.3390/molecules26144338

Afroz, M., Bhuia, M. S., Rahman, M. A., Hasan, R., Islam, T., Islam, M. R., et al. (2024). Anti-diarrheal effect of piperine possibly through the interaction with inflammation inducing enzymes: *in vivo* and *in silico* studies. *Eur. J. Pharmacol.* 965, 176289. doi:10.1016/j.ejphar.2023.176289

Ahmad, Z., Zamhuri, K. F., Yaacob, A., Siong, C. H., Selvarajah, M., Ismail, A., et al. (2012). *In vitro* anti-diabetic activities and chemical analysis of polypeptide-k and oil isolated from seeds of *Momordica charantia* (bitter gourd). *Molecules* 17, 9631–9640. doi:10.3390/molecules17089631

Al-Abbasi, F. A., and Kazmi, I. (2023). Therapeutic role of kaempferol and myricetin in streptozotocin-induced diabetes synergistically via modulation in pancreatic amylase, glycogen storage and insulin secretion. *Mol. Cell. Biochem.* 478, 1927–1937. doi:10.1007/s11010-022-04629-4

Ali, H., Houghton, P., and Soumyanath, A. (2006). α-Amylase inhibitory activity of some Malaysian plants used to treat diabetes; with particular reference to *Phyllanthus amarus*. *J. Ethnopharmacol.* 107, 449–455. doi:10.1016/j.jep.2006.04.004

Al-Yousef, H. M., Hassan, W. H., Abdelaziz, S., Amina, M., Adel, R., and El-Sayed, M. A. (2020). UPLC-ESI-MS/MS profile and antioxidant, cytotoxic, antidiabetic, and antiobesity activities of the aqueous extracts of three different *Hibiscus* species. *J. Chem.* 2020, 1–17. doi:10.1155/2020/6749176

Asaad, G. F., Abdallah, H. M. I., Mohammed, H. S., and Nomier, Y. A. (2021). Hepatoprotective effect of kaempferol glycosides isolated from *Cedrela odorata* L. leaves in albino mice: involvement of Raf/MAPK pathway. *Res. Pharm. Sci.* 16, 370–380. doi:10.4103/1735-5362.319575

Ashraf, H., Moussa, A., Seleem, A., Eldahshan, O. A., and Singab, A.-N. (2020). UPLC-ESI/MS/MS profiling and anti-inflammatory activity of *Gleditsia caspica*. *Arch. pharm. sci. Ain Shams univ.*, 4, 124–134. doi:10.21608/APS.2020.2004.1042

Barros, L., Dueñas, M., Dias, M. I., Sousa, M. J., Santos-Buelga, C., and Ferreira, I. C. (2013). Phenolic profiles of cultivated, *in vitro* cultured and commercial samples of *Melissa officinalis* L. infusions. *Food Chem.* 136, 1–8. doi:10.1016/j.foodchem.2012.07.107

Bastos, D. H., Saldanha, L. A., Catharino, R. R., Sawaya, A., Cunha, I. B., Carvalho, P. O., et al. (2007). Phenolic antioxidants identified by ESI-MS from yerba maté (*Ilex paraguariensis*) and green tea (*Camelia sinensis*) extracts. *Molecules* 12, 423–432. doi:10.3390/12030423

Bellone, M. L., Munoz Camero, C., Chini, M. G., Dal Piaz, F., Hernandez, V., Bifulco, G., et al. (2021). Limonoids from *Guarea guidonia* and *Cedrela odorata*: heat shock protein 90 (Hsp90) modulator properties of chisomicine D. *J. Nat. Prod.* 84, 724–737. doi:10.1021/acs.jnatprod.0c01217

Benayad, Z., Gomez-Cordoves, C., and Es-Safi, N. E. (2014). Characterization of flavonoid glycosides from fenugreek (*Trigonella foenum-graecum*) crude seeds by HPLC-DAD-ESI/MS analysis. *Int. J. Mol. Sci.* 15, 20668–20685. doi:10.3390/ijms151120668

Ben Said, R., Arafa I, H., Usam A, M., Abdullah Sulaiman, A.-A., Kowalczyk, M., Moldoch, J., et al. (2017). Tentative characterization of polyphenolic compounds in the male flowers of *Phoenix dactylifera* by liquid chromatography coupled with mass spectrometry and DFT. *Int. J. Mol. Sci.* 18, 512. doi:10.3390/ijms18030512

Bhuia, M. S., Islam, T., Rokonuzzman, M., Shamsh Prottay, A. A., Akter, F., Hossain, M. I., et al. (2023). Modulatory effects of phytol on the antiemetic property of domperidone, possibly through the D(2) receptor interaction pathway: *in vivo* and *in silico* studies. *Biotech.* 13, 116. doi:10.1007/s13205-023-03520-3

Bystrom, L. M., Lewis, B. A., Brown, D. L., Rodriguez, E., and Obendorf, R. L. (2008). Characterization of phenolics by LC-UV/vis, LC-MS/MS and sugars by GC in *Melicoccus bijugatus* Jacq. 'Montgomery' fruits. *Food Chem.* 111, 1017–1024. doi:10.1016/j.foodchem.2008.04.058

Campos, A. M., Oliveira, F. S., Machado, M. I. L., Matos, F. J., and Braz-Filho, R. (1991). Triterpenes from *Cedrela odorata*. *Phytochemistry* 30, 1225–1229. doi:10.1016/s0031-9422(00)95206-3

Cavers, S., Telford, A., Arenal Cruz, F., Pérez Castañeda, A., Valencia, R., Navarro, C., et al. (2013). Cryptic species and phylogeographical structure in the tree *Cedrela odorata* L. throughout the Neotropics. *J. Biogeogr.* 40, 732–746. doi:10.1111/jbi.12086

Chan, W., Taylor, D., and Aplin, R. (1966). Odoratin, an undecanortriterpenoid from *Cedrela odorata* L. *Chem. Commun.*, 576–577. doi:10.1039/c19660000576

Chan, W. R., Magnus, K., and Mootoo, B. (1967). Extractives from *Cedrela odorata* L. The structure of methyl angolensate. *J. Chem. Soc. C Org.*, 171–177. doi:10.1039/j39670000171

Chaudhury, A., Duvoor, C., Reddy Dendi, V. S., Kraleti, S., Chada, A., Ravilla, R., et al. (2017). Clinical review of antidiabetic drugs: implications for type 2 diabetes mellitus management. *Front. Endocrinol. (Lausanne)* 8, 6. doi:10.3389/fendo.2017.00006

Chen, H. J., Inbaraj, B. S., and Chen, B.-H. (2011). Determination of phenolic acids and flavonoids in *Taraxacum formosanum* Kitam by liquid chromatography-tandem mass spectrometry coupled with a post-column derivatization technique. *Int. J. Mol. Sci.* 13, 260–285. doi:10.3390/ijms13010260

Chen, Q., Zhang, Y., Zhang, W., and Chen, Z. (2011). Identification and quantification of oleanolic acid and ursolic acid in Chinese herbs by liquid chromatography-ion trap mass spectrometry. *Biomed. Chromatogr.* 25, 1381–1388. doi:10.1002/bmc.1614

Choi, C. W., Song, S. B., Oh, J. S., and Kim, Y. H. (2015). Antiproliferation effects of selected Tanzania plants. *Afr. J. Traditional, Complementary Altern. Med.* 12, 96–102. doi:10.21010/ajtcam.v12i2.15

Chowdhury, R., Bhuia, M. S., Al Hasan, M. S., Ansari, S. A., Ansari, I. A., Gurgel, A., et al. (2024). Anticonvulsant effect of (±) citronellal possibly through the GABAergic and voltage-gated sodium channel receptor interaction pathways: *in vivo* and *in silico* studies. *Neurochem. Int.* 175, 105704. doi:10.1016/j.neuint.2024.105704

Chowdhury, R., Bhuia, M. S., Rakib, A. I., Hasan, R., Coutinho, H. D. M., Araújo, I. M., et al. (2023). Assessment of quercetin antiemetic properties: *in vivo* and *in silico* investigations on receptor binding affinity and synergistic effects. *Plants (Basel).* 12, 4189. doi:10.3390/plants12244189

Cunja, V., Mikulic-Petkovsek, M., Stampar, F., and Schmitzer, V. (2014). Compound identification of selected rose species and cultivars: an insight to petal and leaf phenolic profiles. *J. Am. Soc. Hortic. Sci.* 139, 157–166. doi:10.21273/jashs.139.2.157

de Paula, J., Vieira, I. J., Da Silva, M. F. t. d. G., Fo, E. R., Fernandes, J. B., Vieira, P. C., et al. (1997). Sesquiterpenes, triterpenoids, limonoids and flavonoids of *Cedrela odorata* graft and speculations on the induced resistance against *Hypsipyla grandella*. *Phytochemistry* 44, 1449–1454. doi:10.1016/s0031-9422(96)00747-9

Derosa, G., and Maffioli, P. (2012). α-Glucosidase inhibitors and their use in clinical practice. *Arch. Med. Sci.* 8, 899–906. doi:10.5114/aoms.2012.31621

Elhawary, E. A., Mostafa, N. M., Shehata, A. Z., Labib, R. M., and Singab, A. N. B. (2021). Comparative study of selected *Rosa* varieties' metabolites through UPLC-ESI-MS/MS, chemometrics and investigation of their insecticidal activity against *Culex pipiens* L. *Jordan J. Pharm. Sci.*, 14.

ElKhateeb, A., Hussein, S., Salem, M., and El Negoumy, S. (2019). LC-ESI-MS analysis, antitumor and antiviral activities of *Bosica senegalensis* aqueous methanolic extract. *Egypt. J. Chem.* 62, 77–83. doi:10.21608/ejchem.2018.4828.1428

El-Nashar, H. A., Ali, A. A. M., and Salem, Y. H. (2023). Genus pimenta: an updated comprehensive review on botany, distribution, ethnopharmacology, phytochemistry and biological approaches. *Chem. Biodivers.* 20, e202300855. doi:10.1002/cbdv.202300855

El-Nashar, H. A., Mostafa, N. M., El-Shazly, M., and Eldahshan, O. A. (2021a). The role of plant-derived compounds in managing diabetes mellitus: a review of literature from 2014 to 2019. *Curr. Med. Chem.* 28, 4694–4730. doi:10.2174/0929867328999201123194510

El-Nashar, H. A., Eldehna, W. M., Al-Rashood, S. T., Alharbi, A., Eskandrani, R. O., and Aly, S. H. (2021b). GC/MS analysis of essential oil and enzyme inhibitory activities of *Syzygium cumini* (pamposia) grown in Egypt: chemical characterization and molecular docking studies. *Molecules* 26, 6984. doi:10.3390/molecules26226984

El-Nashar, H. A., Taleb, M., EL-Shazly, M., Zhao, C., and Farag, M. A. (2024c). Polysaccharides (pectin, mucilage, and fructan inulin) and their fermented products: a critical analysis of their biochemical, gut interactions, and biological functions as antidiabetic agents. *Phytotherapy Res.* 38, 662–693. doi:10.1002/ptr.8067

El-Nashar, H. A., Mostafa, N. M., Eldahshan, O. A., and Singab, A. N. B. (2022). A new antidiabetic and anti-inflammatory biflavonoid from *Schinus polygama* (Cav.) Cabrera leaves. *Nat. Prod. Res.* 36, 1182–1190. doi:10.1080/14786419.2020.1864365

El-Nashar, H. A., Shabana, E.-S., Kamli, H., Shaikh, A., and Adel, M. (2024a). Chemical composition of leaf essential oil of *Schinopsis lorentzii* and its inhibitory effects against key enzymes relevant to type-2 diabetes: an emphasis on GC-MS chemical profiling and molecular docking studies. *J. Essent. Oil Bear. Plants* 27, 731–743. doi:10.1080/0972060x.2024.2355979

El Sayed, A. M., Ezzat, S. M., El Naggar, M. M., and El Hawary, S. S. (2016a). *In vivo* diabetic wound healing effect and HPLC–DAD–ESI–MS/MS profiling of the methanol extracts of eight *Aloe* species. *Rev. Bras. Farmacogn.* 26, 352–362. doi:10.1016/j.bjp.2016.01.009

El Sayed, A. M., Ezzat, S. M., El Naggar, M. M., and El Hawary, S. S. (2016b). *In vivo* diabetic wound healing effect and HPLC-DAD-ESI-MS/MS profiling of the methanol extracts of eight *Aloe* species. *Rev. Bras. Farmacogn.* 26, 352–362. doi:10.1016/j.bjp.2016.01.009

El-sayed, M., Abbas, F. A., Refaat, S., El-Shafae, A. M., and Fikry, E. (2021). UPLC-ESI-MS/MS profile of the ethyl acetate fraction of aerial parts of *Bougainvillea* 'Scarlett O'Hara' cultivated in Egypt. *Egypt. J. Chem.* 64, 793–806. doi:10.21608/ejchem.2020.45694.2933

El-Sayed, M. A., Al-Gendy, A. A., Hamdan, D. I., and El-Shazly, A. M. (2017). Phytoconstituents, LC-ESI-MS profile, antioxidant and antimicrobial activities of *Citrus x limon* L. Burm. f. cultivar variegated pink lemon. *J. Pharm. Sci. Res.* 9, 375.

Ervina, M. (2020). The recent use of *Swietenia mahagoni* (L.) Jacq. as antidiabetes type 2 phytomedicine: a systematic review. *Heliyon* 6, e03536. doi:10.1016/j.heliyon.2020.e03536

Escobar-Avello, D., Lozano-Castellón, J., Mardones, C., Pérez, A. J., Saéz, V., Riquelme, S., et al. (2019). Phenolic profile of grape canes: novel compounds identified by lc-esi-ltq-orbitrap-ms. *Molecules* 24, 3763. doi:10.3390/molecules24203763

Finch, K. N., Jones, F. A., and Cronn, R. C. (2022). Cryptic species diversity in a widespread neotropical tree genus: the case of *Cedrela odorata*. *Am. J. Bot.* 109, 1622–1640. doi:10.1002/ajb2.16064

Fraternale, D., Ricci, D., Verardo, G., Gorassini, A., Stocchi, V., and Sestili, P. (2015). Activity of *Vitis vinifera* tendrils extract against phytopathogenic fungi. *Nat. Product. Commun.* 10, 1037–1042. doi:10.1177/1934578x1501000661

Galván-Hernández, D. M., Macedo-Villarreal, M. A., Núñez de Cáceres-González, F. F., Sánchez-González, A., and Octavio-Aguilar, P. (2018). Morphological variation of *Cedrela odorata* (Meliaceae): contrast between natural and managed populations. *Acta Botánica mex.*, 157–171. doi:10.21829/abm125.2018.1330

Ghani, A. S., and Badr, W. H. (2020). Diterpenoids profile of *E. paralias* and *E. geniculata* using UPLC-ESI/MS Spectrometry. *Egypt. J. Chem.* 63, 5039–5053. doi:10.21608/ejchem.2020.25113.2486

Ghorbani, A. (2017). Mechanisms of antidiabetic effects of flavonoid rutin. *Biomed. Pharmacother.* 96, 305–312. doi:10.1016/j.biopha.2017.10.001

Giordani, M. A., Collicchio, T. C. M., Ascêncio, S. D., de Oliveira Martins, D. T., Balogun, S. O., Bieski, I. G. C., et al. (2015). Hydroethanolic extract of the inner stem bark of *Cedrela odorata* has low toxicity and reduces hyperglycemia induced by an overload of sucrose and glucose. *J. Ethnopharmacol.* 162, 352–361. doi:10.1016/j.jep.2014.12.059

Godbout, A., and Chiasson, J. L. (2007). Who should benefit from the use of alpha-glucosidase inhibitors? *Curr. Diab Rep.* 7, 333–339. doi:10.1007/s11892-007-0055-x

Gu, L., Kelm, M. A., Hammerstone, J. F., Zhang, Z., Beecher, G., Holden, J., et al. (2003). Liquid chromatographic/electrospray ionization mass spectrometric studies of proanthocyanidins in foods. *J. Mass Spectrom.* 38, 1272–1280. doi:10.1002/jms.541

Hung, H. Y., Qian, K., Morris-Natschke, S. L., Hsu, C. S., and Lee, K. H. (2012). Recent discovery of plant-derived anti-diabetic natural products. *Nat. Prod. Rep.* 29, 580–606. doi:10.1039/c2np00074a

Ibrahim, R. M., El-Halawany, A. M., Saleh, D. O., Naggar, E. M. B. E., El-Shabrawy, A. E.-R. O., and El-Hawary, S. S. (2015). HPLC-DAD-MS/MS profiling of phenolics from *Securigera securidaca* flowers and its anti-hyperglycemic and anti-hyperlipidemic activities. *Rev. Bras. Farmacogn.* 25, 134–141. doi:10.1016/j.bjp.2015.02.008

Jadhav, R., and Puchchakayala, G. (2012). Hypoglycemic and antidiabetic activity of flavonoids: boswellic acid, ellagic acid, quercetin, rutin on streptozotocin-nicotinamide induced type 2 diabetic rats. *Group* 1, 100g.

Jamaddar, S., Sarkar, C., Akter, S., Mubarak, M. S., El-Nashar, H. A., El-Shazly, M., et al. (2023). Brazilin: an updated literature-based review on its promising therapeutic approaches and toxicological studies. *South Afr. J. Bot.* 158, 118–132. doi:10.1016/j.sajb.2023.04.053

Jang, S.-M., Kim, M.-J., Choi, M.-S., Kwon, E.-Y., and Lee, M.-K. (2010). Inhibitory effects of ursolic acid on hepatic polyol pathway and glucose production in streptozotocin-induced diabetic mice. *Metabolism* 59, 512–519. doi:10.1016/j.metabol.2009.07.040

Jang, S.-M., Yee, S.-T., Choi, J., Choi, M.-S., Do, G.-M., Jeon, S.-M., et al. (2009). Ursolic acid enhances the cellular immune system and pancreatic β-cell function in streptozotocin-induced diabetic mice fed a high-fat diet. *Int. Immunopharmacol.* 9, 113–119. doi:10.1016/j.intimp.2008.10.013

Jia, C., Zhu, Y., Zhang, J., Yang, J., Xu, C., and Mao, D. (2017). Identification of glycoside compounds from tobacco by high performance liquid chromatography/ electrospray ionization linear ion-trap tandem mass spectrometry coupled with electrospray ionization orbitrap mass spectrometry. *J. Braz. Chem. Soc.* 28, 629–640. doi:10.21577/0103-5053.20160211

Jung, U. J., Lee, M. K., Park, Y. B., Jeon, S. M., and Choi, M. S. (2006). Antihyperglycemic and antioxidant properties of caffeic acid in db/db mice. *J. Pharmacol. Exp. Ther.* 318, 476–483. doi:10.1124/jpet.106.105163

Kaur, R., Kaur, M., and Singh, J. (2018). Endothelial dysfunction and platelet hyperactivity in type 2 diabetes mellitus: molecular insights and therapeutic strategies. *Cardiovasc. Diabetol.* 17, 121–217. doi:10.1186/s12933-018-0763-3

Kazeem, M. I., Adamson, J. O., and Ogunwande, I. A. (2013). Modes of inhibition of α-amylase and α-glucosidase by aqueous extract of *Morinda lucida* Benth leaf. *Biomed. Res. Int.* 2013, 527570. doi:10.1155/2013/527570

Koul, O. (1983). Feeding deterrence induced by plant limonoids in the larvae of *Spodoptera litura* (F.) (Lepidoptera, Noctuidae). *Z. für Angew. Entomol.* 95, 166–171. doi:10.1111/j.1439-0418.1983.tb02627.x

Kramberger, K., Barlič-Maganja, D., Bandelj, D., Baruca Arbeiter, A., Peeters, K., Miklavčič Višnjevec, A., et al. (2020). HPLC-DAD-ESI-QTOF-MS determination of bioactive compounds and antioxidant activity comparison of the hydroalcoholic and water extracts from two *Helichrysum italicum* species. *Metabolites* 10, 403. doi:10.3390/metabo10100403

Kumari, A., and Kakkar, P. (2008). Screening of antioxidant potential of selected barks of Indian medicinal plants by multiple *in vitro* assays. *Biomed. Environ. Sci.* 21, 24–29. doi:10.1016/s0895-3988(08)60003-3

Lee, H. G., Kim, T. Y., Jeon, J. H., Lee, H. S., Hong, Y. K., and Jin, M. H. (2016). Inhibition of melanogenesis by abietatriene from *Vitex trifolia* leaf oil. *Nat. Product. Sci.* 22, 252–258. doi:10.20307/nps.2016.22.4.252

Lee, J., Yee, S.-T., Kim, J.-J., Choi, M.-S., Kwon, E.-Y., Seo, K.-I., et al. (2010). Ursolic acid ameliorates thymic atrophy and hyperglycemia in streptozotocin–nicotinamide-induced diabetic mice. *Chemico-biological Interact.* 188, 635–642. doi:10.1016/j.cbi.2010.09.019

Li, Y., Li, Y., Chen, N., Feng, L., Gao, J., Zeng, N., et al. (2022). Icariside II exerts anti-type 2 diabetic effect by targeting ppara/γ: involvement of ROS/NF-κB/IRS1 signaling pathway. *Antioxidants* 11, 1705. doi:10.3390/antiox11091705

López-Angulo, G., Montes-Avila, J., Díaz-Camacho, S. P., Vega-Aviña, R., López-Valenzuela, J. Á., and Delgado-Vargas, F. (2018). Comparison of terpene and phenolic profiles of three wild species of *Echeveria* (Crassulaceae). *J. Appl. Bot. Food Qual.* 91, 145–154. doi:10.5073/JABFQ.2018.091.020

Marzouk, M. M., Elkhateeb, A., Latif, R. R. A., Abdel-Hameed, E.-S. S., Kawashty, S. A., and Hussein, S. R. (2019). C-glycosyl flavonoids-rich extract of *Dipcadi erythraeum* Webb and Berthel. bulbs: phytochemical and anticancer evaluations. *J. Appl. Pharm. Sci.* 9, 094–098. doi:10.7324/JAPS.2019.90613

Mugaranja, K. P., and Kulal, A. (2020). Alpha glucosidase inhibition activity of phenolic fraction from *Simarouba glauca*: an *in-vitro, in-silico* and kinetic study. *Heliyon* 6, e04392. doi:10.1016/j.heliyon.2020.e04392

Mukhtar, Y., Galalain, A., and Yunusa, U. (2020). A modern overview on diabetes mellitus: a chronic endocrine disorder. *Eur. J. Biol.* 5, 1–14. doi:10.47672/ejb.409

Muñoz Camero, C., De Leo, M., D'Ambola, M., Gualtieri, M., Braca, A., and De Tommasi, N. (2018). New lignans from *Cedrela odorata* L. Stem bark.

Oboh, G., Ademosun, A. O., Ayeni, P. O., Omojokun, O. S., and Bello, F. (2015). Comparative effect of quercetin and rutin on α-amylase, α-glucosidase, and some pro-oxidant-induced lipid peroxidation in rat pancreas. *Comp. Clin. Pathol.* 24, 1103–1110. doi:10.1007/s00580-014-2040-5

Paritala, V., Chiruvella, K. K., Thammineni, C., Ghanta, R. G., and Mohammed, A. (2015). Phytochemicals and antimicrobial potentials of mahogany family. *Rev. Bras. Farmacogn.* 25, 61–83. doi:10.1016/j.bjp.2014.11.009

Patyra, A., Dudek, M. K., and Kiss, A. K. (2022). LC-DAD–ESI-MS/MS and NMR analysis of conifer wood specialized metabolites. *Cells* 11, 3332. doi:10.3390/cells11203332

Rabie, O., El-Nashar, H. A., Majrashi, T. A., Al-Warhi, T., El Hassab, M. A., Eldehna, W. M., et al. (2023). Chemical composition, seasonal variation and antiaging activities of essential oil from *Callistemon subulatus* leaves growing in Egypt. *J. Enzyme Inhibition Med. Chem.* 38, 2224944. doi:10.1080/14756366.2023.2224944

Rangiah, K., Varalaxmi, B., and Gowda, M. (2016). UHPLC-MS/SRM method for quantification of neem metabolites from leaf extracts of Meliaceae family plants. *Anal. Methods* 8, 2020–2031. doi:10.1039/c5ay03065j

Reed, K. A. (2009). *Identification of phenolic compounds from peanut skin using HPLC-MSn*. Blacksburg, Virginia: Virginia Tech.

Ren, Q., and Long, S.-S. (2017). Chemical identification and quantification of Hu-Gu capsule by UHPLC-Q-TOF-MS and HPLC-DAD. *Rev. Bras. Farmacogn.* 27, 557–563. doi:10.1016/j.bjp.2017.06.002

Rini Vijayan, K. P., and Raghu, A. (2019). Tentative characterization of phenolic compounds in three species of the genus *Embelia* by liquid chromatography coupled with mass spectrometry analysis. *Spectrosc. Lett.* 52, 653–670. doi:10.1080/00387010.2019.1682013

Riyaphan, J., Pham, D.-C., Leong, M. K., and Weng, C.-F. (2021). *In silico* approaches to identify polyphenol compounds as α-glucosidase and α-amylase inhibitors against type-II diabetes. *Biomolecules* 11, 1877. doi:10.3390/biom11121877

Rockenbach, I. I., Jungfer, E., Ritter, C., Santiago-Schübel, B., Thiele, B., Fett, R., et al. (2012). Characterization of flavan-3-ols in seeds of grape pomace by CE, HPLC-DAD-MSn and LC-ESI-FTICR-MS. *Food Res. Int.* 48, 848–855. doi:10.1016/j.foodres.2012.07.001

Saber, F. R., Aly, S. H., Khallaf, M. A., El-Nashar, H. A., Fahmy, N. M., El-Shazly, M., et al. (2023). Hyphaene thebaica (Areceaeae) as a promising functional food: extraction,

analytical techniques, bioactivity, food, and industrial applications. *Food Anal. Methods* 16, 1447–1467. doi:10.1007/s12161-022-02412-1

Saeed, A., Bashir, K., Shah, A. J., Qayyum, R., and Khan, T. (2022). Antihypertensive activity in high salt-induced hypertensive rats and LC-MS/MS-Based phytochemical profiling of *Melia azedarach* L. (Meliaceae) leaves. *Biomed. Res. Int.* 2022, 1–17. doi:10.1155/2022/2791874

Schmeda-Hirschmann, G., Quispe, C., and González, B. (2015). Phenolic profiling of the South American "baylahuen" tea (*Haplopappus* spp., Asteraceae) by HPLC-DAD-ESI-MS. *Molecules* 20, 913–928. doi:10.3390/molecules20010913

Shah, K. H., and Patel, P. M. (2021). Evaluation of antioxidant activity of *Cedrela toona* Roxb. Leaf extracts. *Himal. J. Health Sci.*, 24–31. doi:10.22270/hjhs.v6i1.93

Shen, H., Wang, J., Ao, J., Hou, Y., Xi, M., Cai, Y., et al. (2023). Structure-activity relationships and the underlying mechanism of α-amylase inhibition by hyperoside and quercetin: multi-spectroscopy and molecular docking analyses. *Spectrochimica Acta Part A Mol. Biomol. Spectrosc.* 285, 121797. doi:10.1016/j.saa.2022.121797

Shrestha, A., Rezk, A., Said, I. H., von Glasenapp, V., Smith, R., Ullrich, M. S., et al. (2017). Comparison of the polyphenolic profile and antibacterial activity of the leaves, fruits and flowers of *Rhododendron ambiguum* and *Rhododendron cinnabarinum*. *BMC Res. Notes* 10, 297–311. doi:10.1186/s13104-017-2601-1

Simirgiotis, M. J., Benites, J., Areche, C., and Sepulveda, B. (2015). Antioxidant capacities and analysis of phenolic compounds in three endemic *nolana* species by HPLC-PDA-ESI-MS. *Molecules* 20, 11490–11507. doi:10.3390/molecules200611490

Sobeh, M., ElHawary, E., Peixoto, H., Labib, R. M., Handoussa, H., Swilam, N., et al. (2016). Identification of phenolic secondary metabolites from *Schotia brachypetala* Sond.(Fabaceae) and demonstration of their antioxidant activities in *Caenorhabditis elegans*. *PeerJ* 4, e2404. doi:10.7717/peerj.2404

Takahashi, M., Fuchino, H., Satake, M., Agatsuma, Y., and Sekita, S. (2004). *In vitro* screening of leishmanicidal activity in Myanmar timber extracts. *Biol. Pharm. Bull.* 27, 921–925. doi:10.1248/bpb.27.921

Todirascu-Ciornea, E., El-Nashar, H. A., Mostafa, N. M., Eldahshan, O. A., Boiangiu, R. S., Dumitru, G., et al. (2019). Schinus terebinthifolius essential oil attenuates scopolamine-induced memory deficits via cholinergic modulation and antioxidant properties in a zebrafish model. *Evidence-Based Complementary Altern. Med.* 2019, 5256781. doi:10.1155/2019/5256781

Tundis, R., Loizzo, M. R., and Menichini, F. (2010). Natural products as α-amylase and α-glucosidase inhibitors and their hypoglycaemic potential in the treatment of diabetes: an update. *Mini Rev. Med. Chem.* 10, 315–331. doi:10.2174/138955710791331007

Veitch, N. C., Wright, G. A., and Stevenson, P. C. (1999). Four new tetranortriterpenoids from *Cedrela odorata* associated with leaf rejection by *Exopthalmus jekelianus*. *J. Nat. Prod.* 62, 1260–1263. doi:10.1021/np990151j

Wu, W.-B., Zhang, H., Dong, S.-H., Sheng, L., Wu, Y., Li, J., et al. (2014). New triterpenoids with protein tyrosine phosphatase 1B inhibition from *Cedrela odorata*. *J. Asian Nat. Prod. Res.* 16, 709–716. doi:10.1080/10286020.2014.919281

Xiao, S.-J., Xu, X.-K., Chen, W., Xin, J.-Y., Yuan, W.-L., Zu, X.-P., et al. (2023). Traditional Chinese medicine Euodiae Fructus: botany, traditional use, phytochemistry, pharmacology, toxicity and quality control. *Nat. Prod. Bioprospecting* 13, 6. doi:10.1007/s13659-023-00369-0

Yang, M., Wang, X., Guan, S., Xia, J., Sun, J., Guo, H., et al. (2007). Analysis of triterpenoids in *Ganoderma lucidum* using liquid chromatography coupled with electrospray ionization mass spectrometry. *J. Am. Soc. Mass Spectrom.* 18, 927–939. doi:10.1016/j.jasms.2007.01.012

Ye, M., Guo, D., Ye, G., and Huang, C. (2005). Analysis of homoisoflavonoids in *Ophiopogon japonicus* by HPLC-DAD-ESI-MS. *J. Am. Soc. Mass Spectrom.* 16, 234–243. doi:10.1016/j.jasms.2004.11.007

Zaghloul, E., Handousa, H., Singab, A. N. B., Elmazar, M. M., Ayoub, I. M., and Swilam, N. (2023). Phytoecdysteroids and anabolic effect of *Atriplex dimorphostegia*: UPLC-PDA-MS/MS profiling, *in silico* and *in vivo* models. *Plants* 12, 206. doi:10.3390/plants12010206